A β-catenin-driven switch in TCF/LEF transcription factor binding to DNA target sites promotes commitment of mammalian nephron progenitor cells

Qiuyu Guo[1], Albert Kim[1], Bin Li[3], Andrew Ransick[1], Helena Bugacov[1], Xi Chen[1], Nils Lindstrom[1], Aaron Brown[2], Leif Oxburgh[3], Bing Ren[4], Andrew P. McMahon[1]

1 Department of Stem Cell Biology and Regenerative Medicine, Eli and Edythe Broad-CIRM Center for Regenerative Medicine and Stem Cell Research, Keck School of Medicine of the University of Southern California, CA 90089, USA
2 Center for Molecular Medicine, Maine Medical Center Research Institute, 81 Research Drive, Scarborough, ME 04074, USA
3 The Rogosin Institute, New York, NY, 10065, USA
4 Ludwig Institute for Cancer Research, Department of Cellular and Molecular Medicine, Institute of Genomic Medicine, Moores Cancer Center, University of California San Diego, La Jolla, California, United States of America

Abstract

The canonical Wnt pathway transcriptional co-activator β-catenin regulates self-renewal and differentiation of mammalian nephron progenitor cells (NPCs). We modulated β-catenin levels in NPC cultures using the GSK3 inhibitor CHIR9902 (CHIR) to examine opposing developmental actions of β-catenin. Low CHIR-mediated maintenance and expansion of NPCs is independent of direct engagement of TCF/LEF/β-catenin transcriptional complexes at low CHIR-dependent cell-cycle targets. In contrast, in high CHIR, TCF7/LEF1/β-catenin complexes replaced TCF7L1/TCF7L2 binding on enhancers of differentiation-promoting target genes. Chromosome confirmation studies showed pre-established promoter-enhancer connections to these target genes in NPCs. High CHIR-associated *de novo* looping was observed in positive transcriptional feedback regulation to the canonical Wnt pathway. Thus, β-catenin's direct transcriptional role is restricted to the induction of NPCs where rising β-catenin levels switch inhibitory TCF7L1/TCF7L2 complexes to activating LEF1/TCF7 complexes at primed gene targets poised for rapid initiation of a nephrogenic program.

Introduction

The now classical model of canonical Wnt signaling invokes two transcriptional states (Wiese, Nusse, and van Amerongen 2018; Steinhart and Angers 2018). In the absence of Wnt ligand, HMG box family Tcf transcription factors bind enhancers of Wnt target genes recruiting co-repressors (Tle, Ctbp and others) to silence target gene expression. In the cytoplasm, the transcriptional co-activator β-catenin is phosphorylated by an axin/GSK3β-dependent β-catenin destruction complex, resulting in ubiquitin-mediated proteasomal degradation. Upon Wnt ligand binding to Fzd receptor/Lrp co-receptors on the cell surface, the β-catenin destruction complex is sequestered to the activated receptor protein complex through axin interactions, removing β-catenin from GSK3β-directed, phosphorylation-mediated

degradation (Schaefer and Peifer 2019). As a result of increasing β-catenin levels, β-catenin is free to associate with TCF/LEF DNA binding partners, activating Wnt target gene transcription (Mosimann, Hausmann, and Basler 2009). While evidence suggests all four mammalian Tcf family members are able to functionally interact with both Tle family co-repressors and β-catenin (Brantjes et al. 2001), a variety of studies in a range of biological systems indicate that Tcf7l1 predominantly acts as a repressor, Tcf7l2 as a context-dependent activator or repressor, and Tcf7 and Lef1 as transcriptional activators, of Wnt target gene expression (Lien and Fuchs 2014).

The adult (metanephric) mammalian kidney arises from distinct cell populations within the intermediate mesoderm (McMahon 2016). All nephrons – the repeating functional unit of the kidney – arise from a small pool of a few hundred nephron progenitor cells (NPCs) established at the onset of kidney development (Short et al. 2014; Kobayashi et al. 2008) . The subsequent balance in the maintenance, expansion and commitment of NPCs is critical to ensuring a full complement of nephrons, approximately 14,000 in the mouse and 1 million in the human kidney (Bertram et al. 2011). A reduced nephron endowment has been associated with abnormal kidney function and disease susceptibility (Luyckx and Brenner 2010; McMahon 2016; Bertram et al. 2011). The maintenance and expansion of NPCs is supported by Fgf, Bmp and Wnt signals produced by NPCs or adjacent mesenchymal interstitial progenitor and ureteric epithelial cell types (McMahon 2016). Within this nephrogenic niche, ureteric epithelium-derived Wnt9b is thought to act on NPCs in a β-catenin-dependent transcriptional process to regulate NPC target gene expression and expansion of the nephron progenitor pool (Karner et al. 2011). The removal of *Wnt9b* from the ureteric epithelium and NPC-specific production of β-catenin also results in the failure of NPC differentiation (Carroll et al. 2005), whereas chemical inhibition of GSK3β (Davies and Garrod 1995; Kuure et al. 2007), or genetic activation within NPCs of a β-catenin form insensitive to GSK phosphorylation-mediated proteasomal degradation, leads to Wnt9b-independent ectopic induction of differentiation-promoting gene targets (Park, Valerius, and McMahon 2007). Genomic analysis of β-catenin engagement at TCF/LEF recognition motifs within enhancers linked to genes driving NPC differentiation (Park et al. 2012), and subsequent transgenic studies demonstrating TCF/LEF-dependent activity of cis regulatory elements, provide strong evidence for a canonical Wnt/β-catenin/Tcf regulatory axis (Mosimann, Hausmann, and Basler 2009). Thus, canonical Wnt signaling directs opposing NPC programs: maintenance and expansion of uncommitted NPCs and their commitment to nephron formation.

In this study, we employed an *in vitro* model to investigate the genomic regulatory mechanisms underlying the diverse action of canonical Wnt signaling in NPC programs. In this system, maintenance and expansion of NPCs, or their commitment to a nephrogenic program, are controlled by varying levels of CHIR99021 (Cohen and Goedert, 2004; abbreviated to ‘CHIR’ in the following text) supplemented to a chemically defined nephron progenitor expansion medium (NPEM) (Brown, Muthukrishnan, and

Oxburgh 2015). CHIR binding to Gsk3β inhibits Gsk3β-mediated phosphorylation and proteasomal degradation of β-catenin (Yost et al. 1996; Aberle et al. 1997). Analysis of chromatin interactions and TCF/LEF factor engagement at DNA targets support a model where β-catenin levels act as a key regulatory switch to modify TCF/LEF complex engagement at DNA targets and commitment of NPCs to a nephron-forming program.

Results

Elevated CHIR levels mediate a rapid inductive response in mouse nephron progenitor cells

A low level of CHIR (1.25 μM) is an essential component in NPEM medium supporting the expansion of NPCs while maintaining the nephron-forming competence (Brown et al., 2015). Within 3 days of elevating CHIR levels (3 μM), aggregate NPC cultures show a robust signature of nephron differentiation (Brown, Muthukrishnan, and Oxburgh 2015). To develop this system further for detailed molecular characterization of CHIR/β-catenin-directed transcriptional events, we collected NPCs from E16.5 embryonic kidneys by magnetic-activated cell sorting (MACS; Brown, Muthukrishnan, and Oxburgh 2015). NPCs were cultured in NPEM supplemented with a maintenance level of CHIR (1.25 μM – low CHIR throughout) to promote self-renewal of NPCs. CHIR levels were then titrated to determine an effective concentration for a rapid activation of early target genes of NPC commitment, mirroring *in vivo* responses.

As expected, low CHIR conditions maintained Six2, a key determinant of the NPC state, but did not induce expression of Jag1 (Fig A-C, Figure 1-figure supplement 1B), a Notch pathway ligand activity at early stage of mouse and human NPC commitment (Georgas et al. 2009; Lindstrom, McMahon, et al. 2018). A significant increase of cellular and nuclear β-catenin (Figure 1A, B and Figure 3-figure supplement 2) was observed in 5 μM CHIR (‘high CHIR’ throughout), along with a strong inductive response: Six2 protein level persisted, but there was a robust induction of Jag1(Figure 1A-C), mirroring early inductive events in the pre-tubular aggregate and renal vesicle *in vivo* (Lindstrom, McMahon, et al. 2018; Mugford et al. 2009; Georgas et al. 2009; Xu, Liu, et al. 2014). We adopted this induction condition throughout the study.

Next, we sought to systematically characterize gene expression profiles of NPCs in low and high CHIR conditions by mRNA-seq. Additionally, to explore the effect of low CHIR on NPCs, we generated data removing CHIR from the culture (‘No CHIR’ throughout) (Figure 1-figure supplement 1A). We also examined freshly isolated NPCs prior to culture. Low CHIR maintains expression of transcriptional regulators required for NPC specification and/or maintenance, including *Pax2*, *Wt1*, *Hoxa/d11*, *Sall1* (Figure 1C and Supplementary File 1) (McMahon 2016). In contrast, high CHIR led to a downregulation

of regulators and markers of self-renewing NPCs, including *Six2* (Self et al. 2006), *Cited1* (Mugford et al. 2009), *Osr1* (Xu, Liu, et al. 2014) and *Eya1* (Xu, Wong, et al. 2014), and a concomitant increase in expression of genes associated with induction of nephrogenesis, such as *Wnt4, Jag1, Lhx1* and *Fgf8* (Figure 1C; Park et al., 2007). Trends in gene expression from mRNA-seq were confirmed by RT-qPCR analysis (Figure 1-figure supplement 1B).

To examine biological processes at play in different NPC culture conditions, we performed gene ontology (GO) enrichment analysis of differentially expressed genes (differential expression analysis described in Methods) with DAVID (Huang da, Sherman, and Lempicki 2009). Comparing input NPCs freshly isolated from the kidney cortex with NPC-free cortical preparations ('NFC' throughout), the strong enrichment for NPC-relevant GO terms (Figure 1D, top panel) was consistent with a strong enrichment of Six2+ NPCs (more than 90% of isolated cells were Six2+). When NPCs cultured in high versus low CHIR conditions were compared, a strong enrichment was observed in terms associated with Wnt signaling pathway, as expected, on CHIR-mediated NPC induction (Figure 1D, middle and bottom panels). Although primary NPCs, and their counterpart in low CHIR, showed similar expression patterns for NPC self-renewal and differentiation markers, transcriptome-wide comparison of all samples clustered primary NPCs into a distinct group from NPCs cultured in either low or high CHIR (Figure 1-figure supplement 1C). This is explained by a pronounced metabolic shift in culture where there is a strong enrichment in GO analysis in metabolic processes such as sterol biosynthesis (Figure 1-figure supplement 1D). In addition, freshly isolated NPCs showed a low-level inductive signature reflecting a co-contribution of small numbers of early induced NPCs (expression of *Fgf8, Wnt4, Lhx1, Heyl, Bmp4, Mafb, Podxl*, Figure 1C and Supplementary File 1). Within 24 hours, low CHIR culture stabilized an undifferentiated NPCs signature with the downregulation of induction markers (Figure 1C, S1B and Supplementary File 1). Importantly, these data show NPEM culture establishes a more rigorous model for distinguishing uninduced versus induced NPC responses than is possible with the intrinsic heterogeneity within primary isolates of NPC populations.

CHIR-mediated induction modifies the epigenomic profile of NPCs

To investigate the chromatin landscape regulating NPCs, we integrated chromatin accessibility through ATAC-seq analysis (Buenrostro et al. 2013) with chromatin immunoprecipitation studies examining active (H3K27ac ChIP-seq) and repressive (H3K27me3 ChIP-seq) chromatin features, RNA Pol II recruitment (RNA Pol II Ser5P ChIP-Seq) and RNA-seq expression profiling (Figure 1-figure supplement 1A). Initially, we evaluated enhancers previously validated in transgenic studies (Park et al. 2012) associated with *Six2* expression in uncommitted NPCs (Six2 distal enhancer; Six2DE) and *Wnt4* activation on NPC differentiation (Wnt4 distal enhancer; Wnt4DE). In low CHIR conditions, the Six2DE

shows an open and active configuration: an ATAC-seq peak, flanked by H3K27ac peaks with Pol II engagement at the enhancer and within the gene body. In high CHIR, ATAC-seq, H3K27ac and Pol II ChIP-Seq signals were reduced, correlating with the downregulation of gene expression (Figure 2A). As predicted, the Wnt4DE displayed an opposite trend in the shift from low to high CHIR: the ATAC and H3K27ac ChIP signals increased together with increased Pol II engagement in the gene body. Surprisingly, a marked enhancer specific Pol II ChIP-seq signature was visible in low CHIR NPC maintenance conditions and reduced on initiation of active transcription in high CHIR (Figure 2B).

Having validated the datasets at target loci, we examined the datasets more systematically for broad features of epigenetic regulation. We focused on the differentially accessible regions (DARs) enriched in uncultured NPCs relative to NFC, as they reflect a general NPC-specific signature. NPC-specific DARs were significantly enriched in transcription factor binding sites for Six, Pax and Hox factors consistent with the critical roles of Six1/2, Pax2, and Hox11 paralogues in NPC programs (Figure 2C) (Naiman et al. 2017; Self et al. 2006; Wellik, Hawkes, and Capecchi 2002). Functionally, GO-GREAT analysis (McLean et al. 2010) predicted these regions were enriched near genes linked to kidney development (Figure 2C).

Hierarchical clustering of ATAC-Seq data was used to examine the relationship between CHIR dosage and the open chromatin landscape identifying DARs in NPCs cultured in low and high CHIR conditions (Figure 2-figure supplement 1A). Most of the DARs are distal to the transcriptional start site (TSS) of genes, indicative of enhancer elements (Figure 2-figure supplement 1B). The top two motifs identified in high CHIR-specific DARs were the Jun (AP-1) and TCF/LEF motifs (Figure 2C), supporting a β-catenin driven increase in accessibility through engagement with TCF/LEF factors. Phosphorylated Jun has been detected in both NPCs and differentiate renal vesicles (Muthukrishnan et al. 2015). Further, Jun binds Tcf7l2 to cooperatively activate gene expression in Wnt-dependent intestinal tumors (Nateri, Spencer-Dene, and Behrens 2005). Elevated expression of *Jun*, *Junb* and *Jund* in high CHIR (Supplementary File 1) suggests a potential interplay of Jun family members with β-catenin/Tcf-driven NPC differentiation. Statistical assessment (Supplementary File 2) determined that the Wnt4DE was significantly more accessible in high CHIR vs. low CHIR conditions (peak ID 16567, adjusted p-value = 0.02). The Six2DE showed a trend of greater accessibility in low CHIR vs. high CHIR condition (peak ID 10164, adjusted p-value = 0.13). These observations are consistent with differences in ATAC-Seq data comparing FACS-purified E16 and P2 $Six2^{GFP}$+ cells, where P2 NPCs are thought to have enhanced differentiation capability (Hilliard et al. 2019).

Differential expression and DNA binding of TCF/LEF family members in the regulation of NPC programs

TCF/LEF factors directly bind to DNA and mediate the transcriptional response elicited by Wnt/β-catenin. Studies in other developmental systems have generally documented repressive roles for Tcf7l1 and Tcf7l2, and activating roles for Tcf7 and Lef1 (Lien and Fuchs 2014). To examine the role of TCF/LEF factors directly in NPC maintenance and differentiation, we characterized expression of each of the four members (*Tcf7l1*, *Tcf7l2*, *Tcf7* and *Lef1*). Of the four genes, *Tcf7l1*, *Tcf7l2* and *Tcf7* transcripts were expressed at low (2-10 TPM; *Tcf7l2* and *Tcf7*) or moderate (50 TPM; *Tcf7l1*) levels in low CHIR NPC maintenance conditions. CHIR-mediated induction of NPCs resulted in a significant downregulation of *Tcf7l1* expression, while expression of both *Tcf7* and *Lef1* was markedly upregulated (Figure 3A and S3A-B). The same general trend was observed examining the level of each protein in the nucleus of NPCs through quantitative immunofluorescence (Figure 3B-C) and Western blot (Figure 3-figure supplement 2) analyses. Interestingly, there is a significant decrease in Tcf7l2 protein but not transcript level in high CHIR vs. low CHIR condition, suggesting transcriptionally independent regulation of Tcf7l2 activity. To compare *in vitro* findings with NPCs *in vivo*, single cell RNA-seq (scRNA-Seq) transcriptional profiles were examined in cells isolated from E16.5 kidney cortex. In agreement with *in vitro* data, *Tcf7l1* transcripts were enriched in self-renewing NPCs while *Lef1* levels were elevated in differentiated NPCs, though *Tcf7* and *Tcf7l2* expression levels were relatively low, with little variation between non- and early induced NPC-states (Figure 3-figure supplement 1C-F).

To directly address TCF/LEF target interactions and β-catenin-mediated regulation of NPCs, we generated Lef1, Tcf7, Tcf7l1, Tcf7l2 and β-catenin ChIP-Seq data sets from freshly isolated, uncultured NPCs, and NPCs cultured in low and high CHIR (Figure 1-figure supplement 1A). Further, given the key role for Six2 in NPC maintenance and evidence supporting Six2 engagement in Tcf7l2 and β-catenin containing complexes (Park et al. 2012), we collected Six2 ChIP-seq datasets in the same conditions. Motif discovery of TCF/LEF/β-catenin ChIP-seq binding sites shows highest DNA motif enrichment as the TCF/LEF binding element, indicating a high specificity of the data sets and supporting direct TCF/LEF/β-catenin target interactions (Figure 4-figure supplement 1C). In addition, a Hox motif is highly enriched in TCF/LEF binding sites in both low CHIR and high CHIR conditions consistent with Hox11 paralog regulation of the NPC state (Wellik, Hawkes, and Capecchi 2002; Park et al. 2012). A Runx motif is enriched in TCF/LEF binding sites in high CHIR. *Runx1* expression is upregulated in the same condition (Supplementary File 1), but the significance of possible Runx-dependent regulation remains to be determined.

Consistent with the different levels of each protein in low and high CHIR conditions, Tcf7l1 engagement at DNA targets was reduced on NPC induction, while Tcf7, Lef1 and β-catenin showed a

marked increase in DNA bound sites (Figure 4-figure supplement 1A). In both low and high CHIR conditions, β-catenin association overlapped extensively with the binding of cognate TCF/LEF factors specifically enriched in each condition (Figure 4-figure supplement 1B). In either CHIR condition, motif recovery suggests direct engagement through TCF/LEF binding sites (Figure 4-figure supplement 1C). This is consistent with previous findings in murine intestinal studies that localization of β-catenin is primarily dependent on TCF/LEF factors (Schuijers et al. 2014).

Notably, hierarchical clustering indicates the general feature of TCF/LEF factor binding in low CHIR and high CHIR were distinct and determined by the condition, as different TCF/LEF factors targeted common genomic regions which differ between low CHIR and high CHIR conditions (Figure 4-figure supplement 1D). This observation was most evident examining Tcf7l2. *Tcf7l2* mRNA and protein levels did not vary greatly between low and high CHIR conditions but Tcf7l2 DNA interactions differed significantly (Figure 4-figure supplement 1D). Our previous studies identified (Park et al. 2012) and functionally validated (O'Brien et al. 2018) a Wnt4 distal enhancer (Wnt4DE, Figure 2B) driving *Wnt4* expression in response to NPC induction. This enhancer was shown to interact with Six2, Hoxd11, Osr1 and Wt1, critical determinants of the NPC state (O'Brien et al., 2018). Our data demonstrates Tcf7l1 and Tcf7l2 bind to the Wnt4DE in low CHIR condition but were replaced by Tcf7 and Lef1 in high CHIR conditions (Figure 4A). This switch in TCF/LEF factor binding correlated with activation of *Wnt4* expression, consistent with a potential repressive role for Tcf7l1/Tcf7l2 interactions and activating role for Tcf7/Lef1 engagement (Figure 4A). Interestingly, β-catenin was engaged at the Wnt4DE in low CHIR condition where *Wnt4* was transcriptionally silent, though β-catenin binding at this enhancer was increased on high CHIR induction of NPCs (Figure 4A). In summary, though elevating β-catenin levels through high CHIR stabilization of GSK3β leads to some increase in binding of β-catenin at the *Wnt4* enhancer, a marked switch in the binding signature of TCF/LEF factors is a more striking correlation with subsequent activation of *Wnt4* transcription.

As Tcf7l1 and Lef1 binding best distinguished distinct NPCs' states, we performed a more extensive analysis of these factors. Comparing DNA regions bound by Tcf7l1 in low CHIR and those bound by Lef1 in high CHIR, we observed a significant overlap (p value = 1e-569), though over half were unique to a dataset (Figure 4C). We assigned the Tcf7l1/low CHIR-specific sites (see Supplementary file 3) as set 1 (also 'lost,' as no longer bound by TCF/LEF in high CHIR condition), overlapping sites as set 2 (also 'switch,' as TCF/LEF factors interchange at these sites between low and high CHIR conditions) and Lef1/high CHIR-specific sites as set 3 (also '*de novo*,' as TCF/LEF binding sites arose on elevated CHIR levels). Interestingly, examining motif recovery across sets 1-3 indicated only sets 2 and 3 showed a strong prediction for direct TCF/LEF binding (Figure 4D). Thus, Tcf7l1 likely associates with a large number of DNA regions without direct DNA binding at TCF/LEF response elements. The majority (73%)

of Tcf7l1 sites bound in low CHIR with a predicted TCF/LEF motif overlapped with those bound by Lef1 in high CHIR (Figure 4-figure supplement 2A). In contrast, only 29% of Tcfl71 binding sites without a TCF/LEF motif prediction overlapped with Lef1 bound regions (Figure 4-figure supplement 2A). Thus, switching from a Tcf7l1 to a Lef1-centered DNA interaction at TCF/LEF response elements was a general feature of NPC induction response. Comparing with set 3 ('*de novo*'), set 2 ('switch') sites displayed stronger binding of Tcf7l2, Tcf7, Lef1 and β-catenin, as well as higher level of markers of activated chromatin (ATAC-Seq and H3K27ac ChIP-Seq) in high CHIR condition (Figure 4C). Thus, the data suggests TCF/LEF sites occupied by Tcf7l1 in low CHIR are poised for stronger binding (and therefore activation) by TCF/LEF activators in high CHIR condition. Interestingly, GO GREAT analysis of all 3 sets predicted expected kidney terms such as 'metanephric nephron morphogenesis' or 'renal vesicle morphogenesis' (Figure 4E), consistent with biologically relevant interactions, arguing against artefactual responses to culture or CHIR treatment. More than half of the potential target genes (assigned bioinformatically by GREAT) of set 2 'switch' sites overlaps with those of set 3 '*de novo*' sites (60%; Figure 4G, p = 5.9e-627), although the latter are much broader. For this overlapping group, pre-engagement by Tcf7l1 may increase the likelihood of additional engagement in neighboring regions of DNA by Lef1, and potentially reinforce transcriptional input into a common gene target.

Examining chromatin features and RNA Pol II engagement, we observed stronger enrichment of active enhancer markers (H3K27ac and RNA Pol II) in low CHIR on set 1 sites predicting indirect Tcf7l1 engagement than set 2 sites where Tcf7l1 was predicted to bind DNA directly through TCF/LEF motifs (Figure 4-figure supplement 2E). Thus, direct binding of TCF7L1/TCF7L2 on set 2 sites was associated with putative enhancers in a less active chromatin state in low CHIR condition. Consistent with this view, a direct analysis of the expression of target gene set of set 2 sites showed the highest expression in high CHIR conditions (Figure 4F), suggesting there functions more active in high CHIR. To examine whether elevated β-catenin correlates with chromatin activation, we examined change of active chromatin markers (ATAC-Seq and H3K27ac ChIP-Seq) and RNA Pol II loading on β-catenin bound sites. A dramatic elevation of all these signals in high CHIR condition (Figure 4H) is consistent with β-catenin engagement enhancing an open chromatin, active enhancer signature. Together, the data support the conclusion that high CHIR increased β-catenin association, correlating with switching of TCF/LEF factors at existing active chromatin, *de novo* opening of new chromatin sites, and an active transcription program initiating nephron formation.

β-catenin uses both pre-established and *de novo* enhancer-promoter loops to drive NPC differentiation program

To examine genome organization and chromatin interactions at a higher level in self-renewing and induced NPC, Hi-C analysis (Rao et al. 2014) was performed to characterize global chromatin-chromatin interactions. Further, as CTCF is known to mediate long-range chromatin interactions common across cell types, we integrated a published CTCF ChIP-seq dataset generated from NPCs isolated directly from the developing kidney (O'Brien et al. 2018).

Analysis of two Hi-C data sets, using HiCCUPS within Juicer Tools (Durand et al. 2016), replicated 19,494 low CHIR, and 20,729 high CHIR, chromatin-chromatin interaction loops (Figure 5-figure supplement 1A). Almost half of all loops (40% low CHIR; 44%, high CHIR), including those anchored on TSSs (35% low CHIR; 49% high CHIR), were unique to each culture condition (Figure 5B and Supplementary File 4). Given a focus on chromatin loops responding to β-catenin-mediated induction of NPCs, we examined loops anchored on β-catenin peaks identified in high CHIR conditions. Of the 5,530 β-catenin associated sites in high CHIR condition, 28% (1,573) were located in loop anchors; 41% (647) of these connected to a TSS. Of the 647 peaks looped to TSSs, 57% (371) were connected by 'conserved' loops, shared between low CHIR and high CHIR conditions, the remainder appeared *de novo* under high CHIR conditions (Figure 5A).

To understand the biological consequences of these regulatory events, we identified promoters connected to β-catenin-bound enhancers (Supplementary File 5). Among those connected by conserved loops present in both CHIR conditions, 56 genes were highly expressed in the high CHIR condition (TPM > 5; Supplementary File 5), including *Wnt4*, *Lhx1*, *Emx2*, *Bmp7* and *Cxcr4* which associate with NPC differentiation *in vivo*. Of these, only *Wnt4* enhancer elements have been rigorously defined through transgenic studies (O'Brien et al. 2018). In low CHIR conditions, Six2, Tcf7l1, Tcf7l2 and β-catenin bind to the *Wnt4* distal enhancer (Wnt4DE) while in high CHIR, Tcf7 and Lef1 replace Tcf7 and Tcf7l2, with a concomitant decrease in Six2 and increase in β-catenin association (Figure 5C). Two additional loops further upstream anchor to Ctcf binding sites and loop to the *Wnt4* TSS (Figure 5C). Interestingly, all three loops are stable between low and high CHIR conditions consistent with a pre-determined chromatin organization facilitating rapid activation of a nephron forming inductive program, on switching the TCF/LEF transcriptional input (Figure 5D).

Lef1 was amongst the gene sets defined by highly enriched expression in high CHIR conditions with *de novo* loop formation in high CHIR (Figure 5E and Supplementary File 5). The *Lef1* locus showed no loop connections to the *Lef1* TSS in low CHIR. Further, no TCF/LEF/β-catenin binding was detected, and ATAC-seq and H3K27 acetylation showed only background levels around the *Lef1* locus. In contrast, four interaction loops appeared in high CHIR conditions, one of which was associated with a strong

Lef1/β-catenin interaction site, two mapped to CTCF bound regions (Figure 5E). In high CHIR, a string of LEF1/TCF7/β-catenin binding events accompanied enhanced accessibility (ATAC-seq) and the appearance of an active chromatin signature (H3K27ac) (Figure 5E). These data suggest *de novo* loop formation may follow from *de novo* interaction of LEF1/TCF7/β-catenin binding complexes at the *Lef1* enhancer, in a feedback mechanism driving NPC commitment (Figure 5F).

Discussion

Genetic analysis of mouse models point to a requirement for β-catenin in both the maintenance (Karner et al. 2011) and differentiation (Park, Valerius, and McMahon 2007) of NPCs. Previous studies directly examining β-catenin association in differentiating NPCs showed direct engagement of β-catenin at enhancers regulating expression of differentiation promoting genes such as *Wnt4* (Park et al. 2012). Data here confirmed these earlier findings and extended our understanding through a comprehensive analysis of Wnt-directed transcriptional engagement and epigenetic organization, in a simple *in vitro* model of mammalian NPC programs. TCF/LEF factors are the transcription factors that ultimately mediate the transcriptional response to Wnt signaling. The direct analysis of all four TCF/LEF factors enables several key observations to be made, and conclusions drawn, from the analysis of NPC responses to CHIR modulation of β-catenin levels.

1) In low CHIR, NPC maintenance and expansion conditions, the mitogenic activity mediated through CHIR stimulation of Wnt-signaling appears to be independent of TCF/LEF binding to TCF/LEF motifs in target genes; 2) CHIR-mediated elevation of β-catenin is accompanied by reduced expression of mRNAs for transcriptional inhibitory TCF factors (*Tcf7l1* and *Tcf7l2*), and dramatic increase in expression of mRNAs for activating forms (*Tcf7* and *Lef1*), promoting an inductive program; 3) Direct binding of inhibitory Tcf7l1 and Tcf7l2 engagement at target motifs within putative cis-regulatory elements prefigures engagement of Tcf7 and Lef1 in a chromatin landscape primed for the transcriptional activation of the nephron forming program; 4) High CHIR invokes a switch from inhibitory to activating TCF/LEF engagement at enhancers promoting nephron differentiation consistent with β-catenin controlling TCF/LEF target engagement. 5) In addition to enhancer-promoter loops pre-established in uncommitted NPCs associated with switching of inhibitory to activating TCF/LEF binding signatures on high CHIR induction, TCF/LEF/ β-catenin interactions at *de novo* sites may play additional roles in the inductive process, including positive feedback in the Lef1 program promoting nephrogenesis.

Wnt signaling, β-catenin and TCF/LEF factors in NPC maintenance and expansion

Though genetic evidence supports a direct role for β-catenin in regulating the maintenance and expansion of NPCs, and low CHIR activity is essential for normal NPC expansion *in vitro*, direct analysis of Tcf, Lef and β-catenin engagement does not provide support for a direct transcriptional mechanism mediated through direct TCF/LEF DNA interactions with low CHIR-dependent target genes. We directly examined 16 genes identified in genetic screens *in vivo* to display *Wnt9b*-dependent expression (Karner et al. 2011). Seven of the sixteen showed elevated expression of at least one isoform in low CHIR versus no CHIR (Figure 1-figure supplement 1G and Supplementary File 6) consistent with a Wnt-signaling input. Two of this group, *Pla2g7* and *Tafa5/Fam19a5*, were also reported to be ectopically activated by LiCl stimulation of the Wnt pathway and ectopic activation of β-catenin (Karner et al., 2011). Our data corroborated the up-regulation of *Tafa5*/*Fam19a5* but not *Pla2g7* in high CHIR (Figure 1-figure supplement 1G and Supplementary File 6). However, ChIP-qPCR data arguing for β-catenin engagement around the TSS bindings sites of *Pla2g7* and *Fam19a5/Tafa5* could only be corroborated near one site in our datasets (Figure 4-figure supplement 3). Comparing NPC gene expression profiles in low CHIR versus no CHIR conditions revealed highly significant GO enrichment in cell cycle-related terms (Figure 1-figure supplement 1E), consistent with pro-proliferation roles of β-catenin in self-renewing NPCs. However, among the 85 genes associated with the term 'cell cycle', only one gene shown significant β-catenin association within 500 kb of the TSS in low CHIR (Figure 1-figure supplement 1F), arguing against a scenario that direct transcriptional regulation of these genes through β-catenin engagement.

These findings raise the possibility that β-catenin acts through an alternative transcriptional mechanism. A prominent association of TCF7L1 is observed in low CHIR to DNA regions where the absence of a TCF/LEF motif may suggest indirect means of association, through protein-protein interactions. However, no strong consensus target emerges from examining motif enrichment in this subset of the TCF7L1 binding data (Figure 4D). Alternatively, β-catenin may play an essential, non-transcriptional role that links to control of cell proliferation. TCF-β-catenin nuclear complexes have been reported to oscillate with the cell cycle suggesting potential nuclear roles independent of DNA association (Ding et al. 2014). Further, β-catenin is reported to play an essential, non-transcriptional role in self-renewal of mouse epiblast stem cells (H. Kim et al. 2013). Additionally, CHIR-mediated inhibition of GSK3 outside of β-catenin regulation might play a role. Interestingly, Acebron et al. (2014) have reported that GSK3 inhibition by Wnt ligand administration leads to deubiquitylation and stabilization of target proteins. Importantly, our studies cannot exclude unknown complicating actions of β-catenin or GSK3-independent CHIR-responses. Wnt-ligand mimetics and direct knockout of β-catenin activity offer a promising future approach to confirm CHIR-β-catenin-centered findings in the current study.

In mouse embryonic stem cell (mESC) culture, canonical Wnt signaling, induced by CHIR99021, supports long-term self-renewal of ESCs (Ying et al. 2008). Tcf7l1 has been shown to repress expression of genes involved in stem cell maintenance while Tcf7 and Lef1 activate targets (Yi et al. 2011; Wray et al. 2011) consistent with a classic canonical Wnt transcriptional activation program of stem cell renewal. However, other studies directly analyzing β-catenin interactions at the chromatin level suggest an indirect process where β-catenin may block the negative interplay of Tcf7l1 binding at the Sox motif of Sox-Oct bound stem cell promoting enhancers (Zhang et al., 2013). In this ESC system, β-catenin target sites containing TCF/LEF motif correlate strongly with differentiation promoting targets, consistent with the normal role of β-catenin *in vivo* in regulating gastrulation (Haegel et al. 1995). Addition of a second small molecule (PD03) inhibiting MEK/ERK signaling is essential to block this differentiation promoting activity (Zhang et al. 2013). Further, depletion of both *Tcf7l1* and *Tcf7* are sufficient to maintain Wnt ligand-independent expansion of ESCs, consistent with the implication that β-catenin activation can abrogate the repressive effect of Tcf7l11 independent of an activator Tcf7 (Yi et al. 2011).

In hair follicle stem cells (HFSC), Wnt induces a transition of the stem cells from the quiescent to the proliferative state. Tcf7l1 and Tcf7l2 are preferentially expressed in HFSC, while Lef1 and Tcf7 are preferentially expressed in the differentiated HFSC, i.e. hair germ (HG) cells (Merrill et al. 2001; Lien et al. 2014). TCF7L1/TCF7L2 repress genes involved in HFSC differentiation, which are activated by Tcf7/Lef1, correlating with replacement of TCF7L1/TCF7L2 by Tcf7/Lef1 on relevant enhancers, a close parallel to activity in NPC programs described here (Adam et al. 2018).

Elevating β-catenin leads to activation of Tcf/Lef-bound enhancers

In the Wnt-off state, Tcf factors are known to recruit Groucho family co-repressors (Cavallo et al. 1998) and histone deacetylase (Billin, Thirlwell, and Ayer 2000) to repress Wnt target gene expression.. Upon Wnt ligand stimulation, Groucho is replaced by β-catenin for activation (Brantjes et al. 2001; Daniels and Weis 2005). From evidence *in vitro*, β-catenin has been shown to be able to recruit various chromatin modulators, including histone acetyl transferase (HAT) (Hecht et al. 2000), histone methyl transferase (Sierra et al. 2006), and chromatin remodeler (Barker et al. 2001). Furthermore, through interaction with Pygo and Bcl9 (Kramps et al. 2002; Schwab et al. 2007), as well as direct interaction (S. Kim et al. 2006), β-catenin can form a complex with the Mediator complex, which bridges the Tcf-bound enhancer to RNA Pol II complex at the target gene promoter (Jeronimo and Robert 2017). In addition, Six2 binding at certain TCF/LEF targets in NPCs might also confer a repressive effect; Six2 interacts with histone deacetylation complexes (HDACs), and depletion of the HDACs in NPC elevates *Wnt4* and *Lef1* expression (Liu et al. 2018). Similarly, the repressive chromatin modifier *Ezh1* and *Ezh2* also repress

Wnt4 and Lef1 expression in NPC through maintaining H3K27me3 mark (Liu et al. 2020), although the repressive functions of such chromatin modifiers tend to have broader effects.

The potential for an extended interaction of Tcf7l1 and Tcf7l2 with co-repressors in suppressing the NPC commitment program has not been addressed in this study. However, given the observation that activation of target genes committing NPCs to a nephrogenic program correlates with a switch to Tcf7 and Lef1 engagement, it seems unlikely that removal of a co-repressor input would be sufficient for full activation in the absence of these strong activators. The observed shift in TCF/LEF factor engagement at DNA targets through elevating CHIR levels raises the question of how rising levels of β-catenin might regulate this transcriptional switch. Given a dual role for Tcf7l2 as both a transcriptional repressor and activator in canonical Wnt transcription (Korinek et al. 1997; Chodaparambil et al. 2014; Lien and Fuchs 2014), β-catenin may switch Tcf7l2 to an activator state. Alternatively, low levels of Tcf7 present in low CHIR may be sufficient for β-catenin engagement and transcriptional activation. In this model, binding of a Tcf7-β-catenin complex would be favored over inhibitory TCF complexes. In either scenario, it is likely that the transcriptional up-regulation of *Tcf7* and *Lef1* creates a feed-forward loop to amplify the transcriptional activation response. Distinguishing amongst these possibilities will require effective and sensitive strategies to specifically modify regulatory components in the experimental model system.

Pre-establishment of enhancer-promoter loops prefigures a nephrogenic program

Classical embryological studies have identified two broad categories of inductive processes by which uncommitted stem or progenitor cells make subsequent cell fate choices (Saxén and Sariola 1987). Instructive signaling leads to cells adopting distinct cell fates each determined by the signaling input. In this scenario, cells have multiple fate choices. In contrast, permissive signaling only leads to a single outcome. The observation that nephron anlagen only undergo a restricted nephrogenic response, and no other, to inductive signals, was taken as evidence that nephron progenitor cells are in an inflexible regulatory state, predetermined for kidney formation. Studies in *Drosophila* have indicated that during development, certain enhancer-promoter loops are stable (Ghavi-Helm et al. 2014), i.e., the enhancer-promoter loop is established before the target gene is activated as a mechanism to prime developmentally potent cells to differentiate into pre-destined cell fates.

Analysis of Hi-C data shows enhancer-promoter loops present in low CHIR condition are consistent with NPCs exhibiting a primed genomic state promoting nephron forming programs. Approximately 56% of loops observed in high CHIR were observed in low CHIR. Of these, 70% connected to a TSS (Figure 5B). Example of genes where such ‘conserved’ loops connect TCF/LEF/β-catenin binding events to TSS include a number of genes within the nephrogenic program including *Wnt4*, *Lhx1*, *Emx2*, *Bmp7* and *Cxcr4*. These data are consistent with the concept that at least part of Wnt/β-

catenin activated differentiated program in NPC is primed through enhancer-TSS loop establishment, most likely at the time of specification of the NPC lineage though these remain to be determined. These findings also raise an interesting possibility that Tcf7l1 and Tcf7l2 engagement at such enhancer-promoter regions may maintain the primed state during an extensive period of progenitor expansion, in the course of kidney development. Interestingly, in low CHIR maintenance conditions, the Wnt4DE showed higher levels of PolII association than in high CHIR conditions where *Wnt4* is transcribed (Figure 2A-B), consistent with a stable enhancer/promoter/PolII association in the primed state. Indeed, Tcf7l1 and Tcf7l2 might serve as a platform for assembly of the transcriptional machinery to facilitate target gene activation with a sufficient level of β-catenin. Hi-C studies also identify new loop interactions consistent with *de novo* gene activation, notably in a predicted Lef1 feed-forward loop.

In summary, NPC culture provides a powerful model for deepening a mechanistic understanding of the regulatory processes balancing maintenance, expansion, and commitment of NPCs. This is a valuable model for stem cells as bulk isolation of stem progenitor cells is problematic for many stem/progenitor systems. Further, *in vitro* conditions enabling the controlled switching between stem/progenitor and differentiation programs have only been described for a few of these systems. Given a broad role for Wnt/β-catenin signaling in regulating stem and progenitor cell programs in metazoans, the findings here may have broader significance for Wnt-directed control of organogenesis. Further, Notch and PI3K activity can also drive early nephrogenic responses *in vivo* or *in vitro* (Lindstrom et al. 2015; Boyle et al. 2011). Recent evidence also argues that not all NPCs entering the differentiation program differentiate. A minor subset return to an NPC state after activating Wnt4 suggesting a variability in the epigenetic state amongst differentiating NPCs (Lawlor et al. 2019). The NPC culture model will provide a rigorous analytical platform for future exploration of how distinct pathway activities and variable epigenetic organization determine the induction of mammalian nephrons

Materials and Methods

Key Resources Table				
Reagent type (species) or resource	**Designation**	**Source or reference**	**Identifiers**	**Additional information**
antibody	Rabbit polyclonal anti-Six2	ProteinTech	11562-1-AP; RRID: AB_2189084	ChIP (1:200)

antibody	Mouse monoclonal IgG1 anti-Six2	Abnova	H00010736-M01; RRID: AB_436993	IF (1:1000)
antibody	Rabbit polyclonal anti-β-catenin	ThermoFisher	71-2700; RRID; AB_2533982	ChIP (1:200)
antibody	Rabbit monoclonal anti- non-phopho-β-catenin	Cell Signaling Technology	8814; RRID: AB_11127203	ChIP (1:200), IF (1:500) and Western blot (1:1000)
antibody	Mouse monoclonal anti-Tcf7l1	Santa Cruz	sc-166411; RRID: AB_2302942	IF (1:1000), Western blot (1:1000)
antibody	Rabbit polyclonal anti-Tcf7l1	Thermo Scientific	PA5-40327; RRID: AB_2577173	ChIP (1:200)
antibody	Rabbit monoclonal anti-Tcf7l2	Cell Signaling Technology	2569; RRID: AB_2199816	ChIP (1:200), IF (1:500), Western blot (1:1000)
antibody	Rabbit monoclonal anti-Tcf7	Cell Signaling Technology	2203; RRID: AB_2199302	ChIP (1:200), Western blot (1:1000)
antibody	Rat monoclonal IgG2b anti-Tcf7	R&D Systems	MAB8224	IF (1:100)
antibody	Rabbit monoclonal anti-Lef1	Cell Signaling Technology	2230; RRID: AB_823558	ChIP (1:200), IF (1:500), Western

				blot (1:1000)
antibody	Rabbit monoclonal anti-Histone H3	Abcam	ab1791; RRID: AB_302613	Western blot (1:1000)
antibody	Rabbit monoclonal anti-Histone H3K27ac	Abcam	ab4729; RRID: AB_2118291	ChIP (1:200)
antibody	Mouse monoclonal anti-Histone H3K27me2me3	Active Motif	39536; RRID: AB_2793247	ChIP (1:200)
antibody	Mouse monoclonal anti-Ser5P-RNAPII	Millipore	05-623; RRID: AB_309852	ChIP (1:200)
antibody	Goat polyclonal anti-Jag1	R&D Systems	AF599; RRID: AB_2128257	IF (1:50)
antibody	HRP-conjugated goat anti-mouse IgG1	Thermo Scientific	A10551	Western blot (1:1000)
antibody	HRP-conjugated goat anti-rabbit IgG	Cell Signaling Technology	7074	Western blot (1:1000)
antibody	Alexa647 mouse anti-rat IgG2b	Abcam	ab172335	IF (1:500)
antibody	Alexa555 donkey anti-rabbit IgG	Abcam	ab150074	IF (1:500)

antibody	Alexa488 goat anti-mouse IgG1	Thermo Scientific	A10551	IF (1:500)
commercial assay or kit	SuperScript™ IV VILO™ Master Mix with ezDNase™ Enzyme	Thermo Fisher Scientific	11766050	
commercial assay or kit	Luna® Universal qPCR Master Mix	New England Biolab	M3003	
commercial assay or kit	RNeasy micro kit	Qiagen	74004	
commercial assay or kit	KAPA Stranded mRNA-Seq Kit	Kapa Biosystems	KK8420	
commercial assay or kit	SimpleChIP® Chromatin IP Buffers	Cell Signaling Technology	14231	
commercial assay or kit	protein A/G agarose beads	Thermo Fisher Scientific	20423	
commercial assay or kit	minElute reaction cleanup kit	Qiagen	28204	
commercial assay or kit	SEA block	Thermo Fisher Scientific	107452659	
commercial assay or kit	Thruplex DNA library prep kit	Clontech	R400523	
software, algorithm	Partek® Flow ® platform	Partek (https://www.partek.com/partek-flow/)		

software, algorithm	DESeq2	Love et al., 2014	RRID:SCR_015687	
software, algorithm	DAVID	Huang et al., 2009 (http://david.abcc.ncifcrf.gov/)	RRID:SCR_001881	
software, algorithm	Homer	Heinz et al. 2010 (http://homer.ucsd.edu/)	RRID:SCR_010881	
software, algorithm	QuEST	Valouev et al., 2008		
software, algorithm	GREAT	McLean et al. 2010		

NPC isolation and culture

NPEM formulation and NPC isolation followed the published protocol (Brown et al., 2015). Briefly, kidneys were harvested from fetal mice at E16.5 and placed into cold PBS. As each pair of kidneys was expected to yield approximately half a million NPCs, we routinely used 20 kidneys aiming for approximately 10 million NPCs. After collection, kidneys were washed with HBSS (Life Technologies, 14175-095) then incubated in 2 mL HBSS solution containing 2.5 mg/ml Collagenase A (Roche, 11 088 793 001) and 10 mg/ml Pancreatin (Sigma, P1625) for 15 min at 37 ℃ while rocking on a Nutator platform at 250 rpm. The enzymatic reaction was then terminated by the addition of 0.5 mL of fetal bovine serum (FBS). The resulting supernatant was passed through a 40 μM filter, and then washed with AutoMACS running buffer (Miltenyi, 130-091-221) before spinning down at 500 g for 5 min. The cell pellet, predominantly cell of the cortical nephrogenic zone, was resuspended in 76 μL of AutoMACS running buffer for 10 million cells. NPC enrichment results from the removal of other cell types in the cell suspension using a combination of PE-conjugated antibodies as follows:

anti-CD105-PE (Miltenyi, 130-102-548), 9 μL

anti-CD140-PE (Miltenyi, 130-102-502), 9 μL

anti-Ter119-PE (Miltenyi, 130-102-893), 8 μL

anti-CD326-PE (Miltenyi, 130-102-265), 8 μL

The cells and antibodies were incubated at 4 ℃ for at least 30 min without agitation, then washed 3 times with 1 ml AutoMACS running buffer resuspending cells at each step in 80 μL the same buffer. To remove unwanted cells, 20 μL of anti-PE beads were added to the cell suspension for 30 min at 4 ℃, cells were washed three times in 1ml of running buffer and finally cells resuspended in 0.5 ml of AutoMACS running buffer and sent through the AutoMACS program as described in the published protocol to

remove non-NPC cell types enriching for NPCs (> 85%; Figure 1-figure supplement 1H and see Brown et al., 2015 for additional details).

Ninety-six well NPC culture plates were treated with Matrigel (Corning, 354277) 1:25 in APEL medium and incubated at room temperature in a laminar flow cabinet for cell culture for at least 1 hr. NPC Around 50,000 cells were added to a well for each imaging, RNA-seq or ATAC-seq study. For ChIP-Seq and Hi-C experiments, we cultured 1,500,000 cells in 6-well plates. For all culture experiments data was collected 24 hrs after cell seeding.

Reverse transcription followed by qPCR (RT-qPCR)

Total RNA was reverse-transcribed with SuperScript™ IV VILO™ Master Mix with ezDNase™ Enzyme (cat #: 11766050). qPCR was performed with Luna® Universal qPCR Master Mix Protocol (New England Biolab #M3003) on a Roche LightCycler 96 System. p-values were obtained by performing t-test between replicates of samples indicated. Primers used in RT-qPCR are listed as follows:

Six2:
F: CACCTCCACAAGAATGAAAGCG
R: CTCCGCCTCGATGTAGTGC
Cited1:
F: AACCTTGGAGTGAAGGATCGC
R: GTAGGAGAGCCTATTGGAGATGT
Wnt4:
F: AGACGTGCGAGAAACTCAAAG
R: GGAACTGGTATTGGCACTCCT
Jag1:
F: CCTCGGGTCAGTTTGAGCTG
R: CCTTGAGGCACACTTTGAAGTA
Fgf8:
F: CCGAGGAGGGATCTAAGGAAC
R: CTTCCAAAAGTATCGGTCTCCAC
Lhx1:
F: CCCATCCTGGACCGTTTCC
R: CGCTTGGAGAGATGCCCTG
Pax8:
F: ATGCCTCACAACTCGATCAGA

R: ATGCGTTGACGTACAACTTCT

Tcf7l1:

F: CCCGCTGACACCTCTCATC

R: ACAGTGGGTAATACGGTGACAG

Tcf7l2:

F: AACGAACACAGCGAATGTTTCC

R: CACCTTGTATGTAGCGAACGC

Tcf7:

F: AACTGGCCCGCAAGGAAAG

R: CTCCGGGTAAGTACCGAATGC

Lef1:

F: TGTTTATCCCATCACGGGTGG

R: CATGGAAGTGTCGCCTGACAG

Immunofluorescence staining

To perform immunofluorescence staining, cell cultures were fixed with 4% PFA in PBS for 10 min, then washed with PBS twice before blocking in 1.5% SEA block (ThermoFisher, 107452659) in TBST (0.1% Tween-20 in TBS). After minimally 30 min at room temperature, switched to primary antibody (diluted in blocking reagent) incubation in 4 degree overnight. After washing 3 times with TBST, switched to secondary antibody (diluted in blocking reagent) incubation for minimally 45 min in room temperature, blocking light. This was followed by 3 washes with TBST, then the cells were kept in PBS for confocal imaging. For freshly isolated cells (Figure 1-figure supplement 1H), cells were processed with Cytospin (Thermo Scientific) followed by the procedure described above. Quantification was performed with automatic program created in ImageJ.

Immunoblots

To separate, protein samples containing at least 1 million cells were boiled with β-mercaptol and ran in SDS-PAGE gels casted from 30% Acrylamide/Bis solution 29:1 (Bio-rad, 1610156) using the Mini-PROTEAN® system (Bio-rad). Afterwards, the gel was transferred in Mini Trans-Blot® Cell (Bio-rad) system to PVDF membranes (Immobilon-P, EMD Millipore, IPVH08100). The membrane with protein was blocked with I-block (Applied Biosystem, T2015) in TBST (0.1% TritonX-100 in TBS) at room temperature for 45 min before switching to primary antibody (diluted in blocking reagent) incubation in 4 degree overnight. Subsequently, the membrane was washed 3 times and switched to

secondary antibody incubation (diluted in blocking reagent) for 45 min at room temperature. This was followed by 3 washes with TBST before drying the membrane and adding HRP substrate (Pierce™ ECL Plus Western Blotting Substrate, Thermo, 32132). Finally, the membrane was used on Autoradiography Film (5x7, Blue Devil, Premium, 100 Sheets/Unit, Genesee Scientific/Amazon) to visualize location of protein.

mRNA-Seq and data analysis

50,000 – 100,000 cells were collected for each RNA experiment. RNA was isolated with RNeasy micro kit (Qiagen, #74004). mRNA-Seq libraries were prepared with KAPA Stranded mRNA-Seq Kit (Kapa Biosystems, #KK8420). The libraries were subsequently sequenced with Illumina NextSeq500 model with pair-end 75 bp setting.

mRNA-Seq reads were aligned with STAR (Dobin et al. 2013) to mm10 assembly and quantified with Partek E/M to generate a count table, and finally converted to TPM for representation. All the steps above were implemented in the Partek® Flow® web platform (St. Louis, MO, USA) sponsored by USC Norris Medical Library.

To identify differentially expressed genes, count tables of the two groups of data being compared were processed through DESeq2 (Love, Huber, and Anders 2014) to obtain the negative binomial p values which evaluates the significance of difference by read counts. The differentially expressed genes were defined with the following threshold: TPM > 5, fold change >3, negative binomial p value < 0.05, unless otherwise specified.

Gene Ontology enrichment analysis was performed with DAVID (Huang da, Sherman, and Lempicki 2009).

ChIP-Seq

1. Fixation. Freshly isolated nephron progenitor cells were fixed in 1 mL AutoMACS running buffers (for each 3-5 million cells). Cultured nephron progenitor cells were fixed in NPEM medium before scraping. In both cases, cells were fixed with final 1% formaldehyde (Thermo Fisher Scientific, #28908) for 20 min at room temperature.

2. Chromatin preparation. 3-5 million cells were processed for each chromatin preparation. Chromatin preparation includes cell lysis and nuclei lysis, which were done with SimpleChIP® Sonication Cell and Nuclear Lysis Buffers (Cell Signaling Technology #81804) following manufacturer's instruction.

3. Chromatin fragmentation. For chromatin fragmentation, lysed nuclei were sonicated with Branson Ultrasonics Sonifier S-450, using a double-step microtip. Each sample was re-suspended in 1 mL nuclear lysis buffer in a 15 mL conical tube, embedded in water-filled ice. Sonication was performed at 20% amplitude for 4 min, with 3 secs of interval after each 1 sec of duty time.

4. Immuno-precipitation. 1 million-equivalent fragmented chromatin was used for each immunoprecipitation experiment. Immuno-precipitation was done with SimpleChIP® Chromatin IP Buffers (Cell Signaling Technology #14231) following the manufacturer's instruction, with the following details. The amounts of antibody used were case-dependent. In general, 2 μg or 1:50 to 1:100 antibody was used for each precipitation. Chromatin with antibody were rotated overnight at 4 °C before 1:40 protein A/G agarose beads (Thermo Fisher Scientific, #20423) were added and incubated for another 6 hrs. to overnight. After washing and elution, antibody-precipitated input DNA were purified with minElute reaction cleanup kit (Qiagen, #28204), reconstituting to 35 uL EB buffer.

5. ChIP-qPCR. qPCR was performed with Luna® Universal qPCR Master Mix Protocol (New England Biolab #M3003) on a Roche LightCycler 96 System. For each reaction, 0.5 out of 35 uL ChIP or input DNA was used. The qPCR primers used are listed below:

Six2-DE:

F: ggcccgggatgatacatta

R: cgggtttccaatcaccatag

Wnt4-DE:

F: GACCCATAAGGCAGCATCCA

R: CTTGCTGGGCAGAGATGAA

Non-ChIP:

F: tctgtgtcccatgacgaaaa

R: ggaagtcatgtttggctggt

6. Sequencing. ChIP-Seq libraries were prepared with Thruplex DNA library prep kit (Clontech, #R400523). The libraries were sequenced with Illumina NextSeq500 model using single-end 75 bp setting.

ChIP-Seq data analysis

ChIP-Seq reads were aligned with bowtie2. The alignment files are filtered to remove duplicate reads with Picard (http://broadinstitute.github.io/picard/index.html). Peak calling was performed with MACS2 (Feng et al. 2012) with combined replicate data sets of the ChIP/condition being considered, and using combined replicate input from the same condition as control. To obtain relatively strong peaks, the peaks were first filtered for q-value < 1e-4. Afterwards, the counts of normalized reads were generated

within +/- 250 bp windows of the filtered peaks. To obtain consistent peaks in both replicates, we filtered the ones with > 10-fold enrichment in the +/- 250 bp window in both replicates for downstream analysis. For data shown in Figure S4, the peaks were further filtered for those with fold enrichment > 20 in order to focus on strong peaks. Overlapping peaks were defined as those within 150 bp from each other's center.

For visualization, wiggle tracks were generated with QuEST (Valouev et al. 2008). The intensity of peaks is measured as fold enrichment, which is calculated by the number of reads within the +/- 250 bp window divided by the total mapped reads in the library, normalized to the size of genome. *De novo* Motif discovery and motif scan was performed with Homer (Heinz et al. 2010). Gene Ontology analysis was performed with GREAT (McLean et al. 2010). To determine the overlap of ChIP-Seq peaks, peak centers from the two compared data sets were overlapped, and centers beyond 150 bp from each other were considered as unique sites (Figure 4-figure supplement 1A-B).

ATAC-Seq and data analysis

Each ATAC-Seq experiment was performed with 50,000 cells, following the published protocol (Buenrostro et al. 2013). ATAC-Seq libraries were sequenced with Illumina NextSeq500 model using single-end 75 bp setting.

ATAC-Seq reads were aligned with bowtie2. Peak calling was performed with MACS2 (Feng et al. 2012) without control data. Subsequently, reads from each replicate were counted with Homer (annotatePeak.pl) within +/- 250 bp of peak center. To obtain reproducible peaks, only the ones passing threshold (fold enrichment > 3) in all 3 replicates were retained for downstream analysis.

To identify differentially accessible regions (DARs), we merged reproducible ATAC-Seq peaks in two conditions and counted the reads within +/- 500 bp windows. DESeq2 was applied to identify statistically significantly DARs. The thresholds for identifying DARs are specified in Supplementary File 1.

To perform genome-wide hierarchical clustering, peaks from all replicate data sets in comparison were merged (peaks < 150 bp from each other are combined into one peak taking the midpoint as the new coordinate). Subsequently, ATAC-Seq reads from all samples concerned were counted in +/- 250 bp bins centering on the merged peaks, generating a count table. Hierarchical clustering was generated based on fold enrichment calculated from the count table.

De novo Motif discovery was performed with Homer (Heinz et al., 2010). Gene Ontology analysis was performed with GREAT (McLean et al., 2010).

Hi-C data generation and analysis

We generated about 700 million raw reads for each sample. The reads were aligned by bwa (Li and Durbin 2009), then duplicates were removed with Picard. The Hi-C files were created and loop calling was done with the Juicer Tools (Durand et al. 2016).

To identify loops that are consistently present in both replicates, we extracted loops whose coordinates of anchors are within 10 kb between replicates.

Condition	replicate1	replicate2	overlap
NPC-1.25	35854	39693	12181
NPC-5	36731	40595	12231

To find TSS of genes and peaks connected by loops, we look for peaks that are within 5 kb from center of one of the loop anchors and TSS that are within 15 kb from center of the other loop anchor.

Single-cell RNA-Seq and data analysis

Cortical cells were dissociated from E16.5 kidneys as described in Brown et al., 2015. Single-cell RNA-Seq library was synthesized using the 10X Genomics Chromium platform, with v2 chemistry and reads were mapped with Cell Ranger, as described in Lindstrom et al (Lindstrom, Guo, et al. 2018). Unsupervised clustering of transcriptional profiles, feature plots and dot plots were generated with Seurat v2.3 (Satija et al. 2015). To computationally isolate the nephron lineage, we subset clusters of cells for those highly expressing nephron lineage markers (Six2, Wnt4, Wt1) but not interstitial progenitor cells markers (Foxd1, Meis1, Fat4).

Sample-size estimation

To enable calculation of standard error and finding of statistically differentially expressed genes and differentially accessible regions, we generated 3 samples per condition for RNA-Seq and ATAC-Seq; due to restriction on resource, we generated 2 samples per condition for ChIP-Seq and HiC experiments.

Replicates

Each replicate experiment was performed with a 1-2 months interval. To us, biological replicates are the same assays performed over different litters of mice, and technical replicates are the same biological material (e.g., DNA and RNA) that were assayed multiple times. For sequencing data (stated above) we generated biological replicates only and no technical replicates. For qPCR, we did generate 3 technical replicate per biological replicate, with 3 biological replicates per condition in total. We did not encounter any outliers and did not exclude any data.

Data depository

All of our sequencing data except for the scRNA-Seq data has been submitted to GEO (GSE131119).

Reference

Aberle, H., A. Bauer, J. Stappert, A. Kispert, and R. Kemler. 1997. "beta-catenin is a target for the ubiquitin-proteasome pathway." *EMBO J* 16 (13): 3797-804. https://doi.org/10.1093/emboj/16.13.3797. https://www.ncbi.nlm.nih.gov/pubmed/9233789.

Adam, R. C., H. Yang, Y. Ge, W. H. Lien, P. Wang, Y. Zhao, L. Polak, J. Levorse, S. C. Baksh, D. Zheng, and E. Fuchs. 2018. "Temporal Layering of Signaling Effectors Drives Chromatin Remodeling during Hair Follicle Stem Cell Lineage Progression." *Cell Stem Cell* 22 (3): 398-413.e7. https://doi.org/10.1016/j.stem.2017.12.004. http://dx.doi.org/10.1016/j.stem.2017.12.004.

Barker, N., A. Hurlstone, H. Musisi, A. Miles, M. Bienz, and H. Clevers. 2001. "The chromatin remodelling factor Brg-1 interacts with beta-catenin to promote target gene activation." *Embo j* 20 (17): 4935-43. https://doi.org/10.1093/emboj/20.17.4935. http://dx.doi.org/10.1093/emboj/20.17.4935.

Bertram, J. F., R. N. Douglas-Denton, B. Diouf, M. D. Hughson, and W. E. Hoy. 2011. "Human nephron number: implications for health and disease." *Pediatr Nephrol* 26 (9): 1529-33. https://doi.org/10.1007/s00467-011-1843-8.

Billin, A. N., H. Thirlwell, and D. E. Ayer. 2000. "Beta-catenin-histone deacetylase interactions regulate the transition of LEF1 from a transcriptional repressor to an activator." *Mol Cell Biol* 20 (18): 6882-90. http://dx.doi.org/.

Boyle, S. C., M. Kim, M. T. Valerius, A. P. McMahon, and R. Kopan. 2011. "Notch pathway activation can replace the requirement for Wnt4 and Wnt9b in mesenchymal-to-epithelial transition of nephron stem cells." *Development* 138 (19): 4245-54. https://doi.org/10.1242/dev.070433. http://dx.doi.org/10.1242/dev.070433.

Brantjes, H., J. Roose, M. van De Wetering, and H. Clevers. 2001. "All Tcf HMG box transcription factors interact with Groucho-related co-repressors." *Nucleic Acids Res* 29 (7): 1410-9. http://dx.doi.org/.

Brown, A. C., S. D. Muthukrishnan, and L. Oxburgh. 2015. "A synthetic niche for nephron progenitor cells." *Dev Cell* 34 (2): 229-41. https://doi.org/10.1016/j.devcel.2015.06.021.

Buenrostro, J. D., P. G. Giresi, L. C. Zaba, H. Y. Chang, and W. J. Greenleaf. 2013. "Transposition of native chromatin for fast and sensitive epigenomic profiling of open chromatin, DNA-binding proteins and nucleosome position." *Nat Methods* 10 (12): 1213-8. https://doi.org/10.1038/nmeth.2688.

Carroll, T. J., J. S. Park, S. Hayashi, A. Majumdar, and A. P. McMahon. 2005. "Wnt9b plays a central role in the regulation of mesenchymal to epithelial transitions underlying organogenesis of the mammalian urogenital system." *Dev Cell* 9 (2): 283-92. https://doi.org/10.1016/j.devcel.2005.05.016.

Cavallo, R. A., R. T. Cox, M. M. Moline, J. Roose, G. A. Polevoy, H. Clevers, M. Peifer, and A. Bejsovec. 1998. "Drosophila Tcf and Groucho interact to repress Wingless signalling

activity." *Nature* 395 (6702): 604-8. https://doi.org/10.1038/26982. http://dx.doi.org/10.1038/26982.

Chodaparambil, J. V., K. T. Pate, M. R. Hepler, B. P. Tsai, U. M. Muthurajan, K. Luger, M. L. Waterman, and W. I. Weis. 2014. "Molecular functions of the TLE tetramerization domain in Wnt target gene repression." *Embo j* 33 (7): 719-31. https://doi.org/10.1002/embj.201387188. http://dx.doi.org/10.1002/embj.201387188.

Daniels, D. L., and W. I. Weis. 2005. "Beta-catenin directly displaces Groucho/TLE repressors from Tcf/Lef in Wnt-mediated transcription activation." *Nat Struct Mol Biol* 12 (4): 364-71. https://doi.org/10.1038/nsmb912.

Davies, J. A., and D. R. Garrod. 1995. "Induction of early stages of kidney tubule differentiation by lithium ions." *Dev Biol* 167 (1): 50-60. https://doi.org/10.1006/dbio.1995.1006. https://www.ncbi.nlm.nih.gov/pubmed/7851662.

Ding, Y., S. Su, W. Tang, X. Zhang, S. Chen, G. Zhu, J. Liang, W. Wei, Y. Guo, L. Liu, Y. G. Chen, and W. Wu. 2014. "Enrichment of the β-catenin-TCF complex at the S and G2 phases ensures cell survival and cell cycle progression." *J Cell Sci* 127 (Pt 22): 4833-45. https://doi.org/10.1242/jcs.146977. https://www.ncbi.nlm.nih.gov/pubmed/25236602.

Dobin, A., C. A. Davis, F. Schlesinger, J. Drenkow, C. Zaleski, S. Jha, P. Batut, M. Chaisson, and T. R. Gingeras. 2013. "STAR: ultrafast universal RNA-seq aligner." *Bioinformatics* 29 (1): 15-21. https://doi.org/10.1093/bioinformatics/bts635. http://dx.doi.org/10.1093/bioinformatics/bts635.

Durand, N. C., M. S. Shamim, I. Machol, S. S. Rao, M. H. Huntley, E. S. Lander, and E. L. Aiden. 2016. "Juicer Provides a One-Click System for Analyzing Loop-Resolution Hi-C Experiments." *Cell Syst* 3 (1): 95-8. https://doi.org/10.1016/j.cels.2016.07.002. http://dx.doi.org/10.1016/j.cels.2016.07.002.

Feng, Jianxing, Tao Liu, Bo Qin, Yong Zhang, and Xiaole Shirley Liu. 2012. "Identifying ChIP-seq enrichment using MACS." *Nature Protocols* 7 (9): 1728. https://doi.org/doi:10.1038/nprot.2012.101. https://www.nature.com/articles/nprot.2012.101.

Georgas, K., B. Rumballe, M. T. Valerius, H. S. Chiu, R. D. Thiagarajan, E. Lesieur, B. J. Aronow, E. W. Brunskill, A. N. Combes, D. Tang, D. Taylor, S. M. Grimmond, S. S. Potter, A. P. McMahon, and M. H. Little. 2009. "Analysis of early nephron patterning reveals a role for distal RV proliferation in fusion to the ureteric tip via a cap mesenchyme-derived connecting segment." *Dev Biol* 332 (2): 273-86. https://doi.org/10.1016/j.ydbio.2009.05.578. http://dx.doi.org/10.1016/j.ydbio.2009.05.578.

Ghavi-Helm, Y., F. A. Klein, T. Pakozdi, L. Ciglar, D. Noordermeer, W. Huber, and E. E. Furlong. 2014. "Enhancer loops appear stable during development and are associated with paused polymerase." *Nature* 512 (7512): 96-100. https://doi.org/10.1038/nature13417. http://dx.doi.org/10.1038/nature13417.

Haegel, H., L. Larue, M. Ohsugi, L. Fedorov, K. Herrenknecht, and R. Kemler. 1995. "Lack of beta-catenin affects mouse development at gastrulation." https://dev.biologists.org/content/121/11/3529.short.

Hecht, A., K. Vleminckx, M. P. Stemmler, F. van Roy, and R. Kemler. 2000. "The p300/CBP acetyltransferases function as transcriptional coactivators of beta-catenin in vertebrates." *Embo j* 19 (8): 1839-50. https://doi.org/10.1093/emboj/19.8.1839. http://dx.doi.org/10.1093/emboj/19.8.1839.

Heinz, S., C. Benner, N. Spann, E. Bertolino, Y. C. Lin, P. Laslo, J. X. Cheng, C. Murre, H. Singh, and C. K. Glass. 2010. "Simple combinations of lineage-determining transcription factors prime cis-regulatory elements required for macrophage and B cell identities." *Mol Cell* 38 (4): 576-89. https://doi.org/10.1016/j.molcel.2010.05.004. http://dx.doi.org/10.1016/j.molcel.2010.05.004.

Hilliard, S., R. Song, H. Liu, C. H. Chen, Y. Li, M. Baddoo, E. Flemington, A. Wanek, J. Kolls, Z. Saifudeen, and S. S. El-Dahr. 2019. "Defining the dynamic chromatin landscape of mouse nephron progenitors." *Biol Open* 8 (5). https://doi.org/10.1242/bio.042754. https://www.ncbi.nlm.nih.gov/pubmed/31064740.

Huang da, W., B. T. Sherman, and R. A. Lempicki. 2009. "Systematic and integrative analysis of large gene lists using DAVID bioinformatics resources." *Nat Protoc* 4 (1): 44-57. https://doi.org/10.1038/nprot.2008.211. http://dx.doi.org/10.1038/nprot.2008.211.

Jeronimo, C., and F. Robert. 2017. "The Mediator Complex: At the Nexus of RNA Polymerase II Transcription." *Trends Cell Biol* 27 (10): 765-783. https://doi.org/10.1016/j.tcb.2017.07.001. http://dx.doi.org/10.1016/j.tcb.2017.07.001.

Karner, C. M., A. Das, Z. Ma, M. Self, C. Chen, L. Lum, G. Oliver, and T. J. Carroll. 2011. "Canonical Wnt9b signaling balances progenitor cell expansion and differentiation during kidney development." *Development* 138 (7): 1247-57. https://doi.org/10.1242/dev.057646. http://dx.doi.org/10.1242/dev.057646.

Kim, H., J. Wu, S. Ye, C. I. Tai, X. Zhou, H. Yan, P. Li, M. Pera, and Q. L. Ying. 2013. "Modulation of β-catenin function maintains mouse epiblast stem cell and human embryonic stem cell self-renewal." *Nat Commun* 4: 2403. https://doi.org/10.1038/ncomms3403. https://www.ncbi.nlm.nih.gov/pubmed/23985566.

Kim, S., X. Xu, A. Hecht, and T. G. Boyer. 2006. "Mediator is a transducer of Wnt/beta-catenin signaling." *J Biol Chem* 281 (20): 14066-75. https://doi.org/10.1074/jbc.M602696200. http://dx.doi.org/10.1074/jbc.M602696200.

Kobayashi, A., M. T. Valerius, J. W. Mugford, T. J. Carroll, M. Self, G. Oliver, and A. P. McMahon. 2008. "Six2 defines and regulates a multipotent self-renewing nephron progenitor population throughout mammalian kidney development." *Cell Stem Cell* 3 (2): 169-81. https://doi.org/10.1016/j.stem.2008.05.020.

Korinek, V., N. Barker, P. J. Morin, D. van Wichen, R. de Weger, K. W. Kinzler, B. Vogelstein, and H. Clevers. 1997. "Constitutive transcriptional activation by a beta-catenin-Tcf complex in APC-/- colon carcinoma." *Science* 275 (5307): 1784-7. http://dx.doi.org/.

Kramps, T., O. Peter, E. Brunner, D. Nellen, B. Froesch, S. Chatterjee, M. Murone, S. Zullig, and K. Basler. 2002. "Wnt/wingless signaling requires BCL9/legless-mediated recruitment of pygopus to the nuclear beta-catenin-TCF complex." *Cell* 109 (1): 47-60. http://dx.doi.org/.

Kuure, S., A. Popsueva, M. Jakobson, K. Sainio, and H. Sariola. 2007. "Glycogen synthase kinase-3 inactivation and stabilization of beta-catenin induce nephron differentiation in isolated mouse and rat kidney mesenchymes." *J Am Soc Nephrol* 18 (4): 1130-9. https://doi.org/10.1681/ASN.2006111206. https://www.ncbi.nlm.nih.gov/pubmed/17329570.

Lawlor, K. T., L. Zappia, J. Lefevre, J. S. Park, N. A. Hamilton, A. Oshlack, M. H. Little, and A. N. Combes. 2019. "Nephron progenitor commitment is a stochastic process influenced by cell migration." *Elife* 8. https://doi.org/10.7554/eLife.41156. https://www.ncbi.nlm.nih.gov/pubmed/30676318.

Li, H., and R. Durbin. 2009. "Fast and accurate short read alignment with Burrows-Wheeler transform." *Bioinformatics* 25 (14): 1754-60. https://doi.org/10.1093/bioinformatics/btp324. http://dx.doi.org/10.1093/bioinformatics/btp324.

Lien, W. H., and E. Fuchs. 2014. "Wnt some lose some: transcriptional governance of stem cells by Wnt/beta-catenin signaling." *Genes Dev* 28 (14): 1517-32. https://doi.org/10.1101/gad.244772.114. http://dx.doi.org/10.1101/gad.244772.114.

Lien, W. H., L. Polak, M. Lin, K. Lay, D. Zheng, and E. Fuchs. 2014. "In vivo transcriptional governance of hair follicle stem cells by canonical Wnt regulators." *Nat Cell Biol* 16 (2): 179-90. https://doi.org/10.1038/ncb2903. http://dx.doi.org/10.1038/ncb2903.

Lindstrom, N. O., J. Guo, A. D. Kim, T. Tran, Q. Guo, G. De Sena Brandine, A. Ransick, R. K. Parvez, M. E. Thornton, L. Baskin, B. Grubbs, J. A. McMahon, A. D. Smith, and A. P. McMahon. 2018. "Conserved and Divergent Features of Mesenchymal Progenitor Cell Types within the Cortical Nephrogenic Niche of the Human and Mouse Kidney." *J Am Soc Nephrol* 29 (3): 806-824. https://doi.org/10.1681/asn.2017080890. http://dx.doi.org/10.1681/asn.2017080890.

Lindstrom, N. O., M. L. Lawrence, S. F. Burn, J. A. Johansson, E. R. Bakker, R. A. Ridgway, C. H. Chang, M. J. Karolak, L. Oxburgh, D. J. Headon, O. J. Sansom, R. Smits, J. A. Davies, and P. Hohenstein. 2015. "Integrated beta-catenin, BMP, PTEN, and Notch signalling patterns the nephron." *Elife* 3: e04000. https://doi.org/10.7554/eLife.04000. http://dx.doi.org/10.7554/eLife.04000.

Lindstrom, N. O., J. A. McMahon, J. Guo, T. Tran, Q. Guo, E. Rutledge, R. K. Parvez, G. Saribekyan, R. E. Schuler, C. Liao, A. D. Kim, A. Abdelhalim, S. W. Ruffins, M. E. Thornton, L. Baskin, B. Grubbs, C. Kesselman, and A. P. McMahon. 2018. "Conserved and Divergent Features of Human and Mouse Kidney Organogenesis." *J Am Soc Nephrol* 29 (3): 785-805. https://doi.org/10.1681/asn.2017080887. http://dx.doi.org/10.1681/asn.2017080887.

Liu, H., S. Chen, X. Yao, Y. Li, C. H. Chen, J. Liu, Z. Saifudeen, and S. S. El-Dahr. 2018. "Histone deacetylases 1 and 2 regulate the transcriptional programs of nephron progenitors and renal vesicles." *Development* 145 (10). https://doi.org/10.1242/dev.153619. https://www.ncbi.nlm.nih.gov/pubmed/29712641.

Liu, H., S. Hilliard, E. Kelly, C. H. Chen, Z. Saifudeen, and S. S. El-Dahr. 2020. "The polycomb proteins EZH1 and EZH2 co-regulate chromatin accessibility and nephron progenitor cell lifespan in mice." *J Biol Chem* 295 (33): 11542-11558. https://doi.org/10.1074/jbc.RA120.013348. https://www.ncbi.nlm.nih.gov/pubmed/32554463.

Love, Michael I, Wolfgang Huber, and Simon Anders. 2014. "Moderated estimation of fold change and dispersion for RNA-seq data with DESeq2." *Genome Biology* 15 (12): 550. https://doi.org/doi:10.1186/s13059-014-0550-8. https://genomebiology.biomedcentral.com/articles/10.1186/s13059-014-0550-8.

Luyckx, V. A., and B. M. Brenner. 2010. "The clinical importance of nephron mass." *J Am Soc Nephrol* 21 (6): 898-910. https://doi.org/10.1681/asn.2009121248. http://dx.doi.org/10.1681/asn.2009121248.

McLean, C. Y., D. Bristor, M. Hiller, S. L. Clarke, B. T. Schaar, C. B. Lowe, A. M. Wenger, and G. Bejerano. 2010. "GREAT improves functional interpretation of cis-regulatory regions." *Nat Biotechnol* 28 (5): 495-501. https://doi.org/10.1038/nbt.1630.

McMahon, A. P. 2016. "Development of the Mammalian Kidney." *Curr Top Dev Biol* 117: 31-64. https://doi.org/10.1016/bs.ctdb.2015.10.010.

Merrill, Bradley J., Uri Gat, Ramanuj DasGupta, and Elaine Fuchs. 2001. "Tcf3 and Lef1 regulate lineage differentiation of multipotent stem cells in skin." https://doi.org/10.1101/gad.891401. http://genesdev.cshlp.org/content/15/13/1688.short.

Mosimann, C., G. Hausmann, and K. Basler. 2009. "Beta-catenin hits chromatin: regulation of Wnt target gene activation." *Nat Rev Mol Cell Biol* 10 (4): 276-86. https://doi.org/10.1038/nrm2654. http://dx.doi.org/10.1038/nrm2654.

Mugford, J. W., J. Yu, A. Kobayashi, and A. P. McMahon. 2009. "High-resolution gene expression analysis of the developing mouse kidney defines novel cellular compartments within the nephron progenitor population." *Dev Biol* 333 (2): 312-23. https://doi.org/10.1016/j.ydbio.2009.06.043.

Muthukrishnan, S. D., X. Yang, R. Friesel, and L. Oxburgh. 2015. "Concurrent BMP7 and FGF9 signalling governs AP-1 function to promote self-renewal of nephron progenitor cells." *Nat Commun* 6: 10027. https://doi.org/10.1038/ncomms10027. http://dx.doi.org/10.1038/ncomms10027.

Naiman, Natalie, Kaoru Fujioka, Mari Fujino, M. Todd Valerius, S. Steven Potter, Andrew P. McMahon, and Akio Kobayashi. 2017. "Repression of Interstitial Identity in Nephron Progenitor Cells by Pax2 Establishes the Nephron-Interstitium Boundary during Kidney Development." *Developmental Cell* 41 (4): 349-365.e3. https://doi.org/https://doi.org/10.1016/j.devcel.2017.04.022. http://www.sciencedirect.com/science/article/pii/S1534580717303489.

Nateri, A. S., B. Spencer-Dene, and A. Behrens. 2005. "Interaction of phosphorylated c-Jun with TCF4 regulates intestinal cancer development." *Nature* 437 (7056): 281-5. https://doi.org/10.1038/nature03914. http://dx.doi.org/10.1038/nature03914.

O'Brien, L. L., Q. Guo, E. Bahrami-Samani, J. S. Park, S. M. Hasso, Y. J. Lee, A. Fang, A. D. Kim, J. Guo, T. M. Hong, K. A. Peterson, S. Lozanoff, R. Raviram, B. Ren, B. Fogelgren, A. D. Smith, A. Valouev, and A. P. McMahon. 2018. "Transcriptional regulatory control of mammalian nephron progenitors revealed by multi-factor cistromic analysis and genetic studies." *PLoS Genet* 14 (1): e1007181. https://doi.org/10.1371/journal.pgen.1007181. http://dx.doi.org/10.1371/journal.pgen.1007181.

Park, J. S., W. Ma, L. L. O'Brien, E. Chung, J. J. Guo, J. G. Cheng, M. T. Valerius, J. A. McMahon, W. H. Wong, and A. P. McMahon. 2012. "Six2 and Wnt regulate self-renewal and commitment of nephron progenitors through shared gene regulatory networks." *Dev Cell* 23 (3): 637-51. https://doi.org/10.1016/j.devcel.2012.07.008.

Park, J. S., M. T. Valerius, and A. P. McMahon. 2007. "Wnt/beta-catenin signaling regulates nephron induction during mouse kidney development." *Development* 134 (13): 2533-9. https://doi.org/10.1242/dev.006155. http://dx.doi.org/10.1242/dev.006155.

Rao, S. S., M. H. Huntley, N. C. Durand, E. K. Stamenova, I. D. Bochkov, J. T. Robinson, A. L. Sanborn, I. Machol, A. D. Omer, E. S. Lander, and E. L. Aiden. 2014. "A 3D map of the human genome at kilobase resolution reveals principles of chromatin looping." *Cell* 159 (7): 1665-80. https://doi.org/10.1016/j.cell.2014.11.021. http://dx.doi.org/10.1016/j.cell.2014.11.021.

Satija, R., J. A. Farrell, D. Gennert, A. F. Schier, and A. Regev. 2015. "Spatial reconstruction of single-cell gene expression data." *Nat Biotechnol* 33 (5): 495-502. https://doi.org/10.1038/nbt.3192. http://dx.doi.org/10.1038/nbt.3192.

Saxén, L., and H. Sariola. 1987. "Early organogenesis of the kidney." *Pediatr Nephrol* 1 (3): 385-92. https://doi.org/10.1007/BF00849241. https://www.ncbi.nlm.nih.gov/pubmed/3153305.

Schaefer, K. N., and M. Peifer. 2019. "Wnt/Beta-Catenin Signaling Regulation and a Role for Biomolecular Condensates." *Dev Cell* 48 (4): 429-444. https://doi.org/10.1016/j.devcel.2019.01.025. http://dx.doi.org/10.1016/j.devcel.2019.01.025.

Schuijers, J., M. Mokry, P. Hatzis, E. Cuppen, and H. Clevers. 2014. "Wnt-induced transcriptional activation is exclusively mediated by TCF/LEF." *EMBO J* 33 (2): 146-56. https://doi.org/10.1002/embj.201385358. https://www.ncbi.nlm.nih.gov/pubmed/24413017.

Schwab, K. R., L. T. Patterson, H. A. Hartman, N. Song, R. A. Lang, X. Lin, and S. S. Potter. 2007. "Pygo1 and Pygo2 roles in Wnt signaling in mammalian kidney development." *BMC Biol* 5: 15. https://doi.org/10.1186/1741-7007-5-15. https://www.ncbi.nlm.nih.gov/pubmed/17425782.

Self, Michelle, Oleg V Lagutin, Beth Bowling, Jaime Hendrix, Yi Cai, Gregory R Dressler, and Guillermo Oliver. 2006. "Six2 is required for suppression of nephrogenesis and progenitor renewal in the developing kidney." https://doi.org/10.1038/sj.emboj.7601381. http://emboj.embopress.org/content/25/21/5214.

Short, Kieran M, Alexander N Combes, James Lefevre, Adler L Ju, Kylie M Georgas, Timothy Lamberton, Oliver Cairncross, Bree A Rumballe, Andrew P McMahon, Nicholas A Hamilton, Ian M Smyth, and Melissa H Little. 2014. "Global Quantification of Tissue Dynamics in the Developing Mouse Kidney." *Developmental Cell* 29 (2): 188-202. https://doi.org/https://doi.org/10.1016/j.devcel.2014.02.017. http://www.sciencedirect.com/science/article/pii/S1534580714001336.

Sierra, J., T. Yoshida, C. A. Joazeiro, and K. A. Jones. 2006. "The APC tumor suppressor counteracts beta-catenin activation and H3K4 methylation at Wnt target genes." *Genes Dev* 20 (5): 586-600. https://doi.org/10.1101/gad.1385806. http://dx.doi.org/10.1101/gad.1385806.

Steinhart, Zachary, and Stephane Angers. 2018. "Wnt signaling in development and tissue homeostasis." https://doi.org/10.1242/dev.146589. https://dev.biologists.org/content/145/11/dev146589?utm_source=TrendMD&utm_campaign=Development_TrendMD_0&utm_content=dev146589&utm_medium=cpc.

Valouev, A., D. S. Johnson, A. Sundquist, C. Medina, E. Anton, S. Batzoglou, R. M. Myers, and A. Sidow. 2008. "Genome-wide analysis of transcription factor binding sites based on ChIP-Seq data." *Nat Methods* 5 (9): 829-34. https://doi.org/10.1038/nmeth.1246.

Wellik, D. M., P. J. Hawkes, and M. R. Capecchi. 2002. "Hox11 paralogous genes are essential for metanephric kidney induction." *Genes Dev* 16 (11): 1423-32. https://doi.org/10.1101/gad.993302.

Wiese, K. E., R. Nusse, and R. van Amerongen. 2018. "Wnt signalling: conquering complexity." *Development* 145 (12). https://doi.org/10.1242/dev.165902. http://dx.doi.org/10.1242/dev.165902.

Wray, J., T. Kalkan, S. Gomez-Lopez, D. Eckardt, A. Cook, R. Kemler, and A. Smith. 2011. "Inhibition of glycogen synthase kinase-3 alleviates Tcf3 repression of the pluripotency network and increases embryonic stem cell resistance to differentiation." *Nat Cell Biol* 13 (7): 838-45. https://doi.org/10.1038/ncb2267. https://www.ncbi.nlm.nih.gov/pubmed/21685889.

Xu, J., H. Liu, J. S. Park, Y. Lan, and R. Jiang. 2014. "Osr1 acts downstream of and interacts synergistically with Six2 to maintain nephron progenitor cells during kidney organogenesis." *Development* 141 (7): 1442-52.

Xu, J., E. Y. Wong, C. Cheng, J. Li, M. T. Sharkar, C. Y. Xu, B. Chen, J. Sun, D. Jing, and P. X. Xu. 2014. "Eya1 interacts with Six2 and Myc to regulate expansion of the nephron progenitor pool during nephrogenesis." *Dev Cell* 31 (4): 434-47.

Yi, F., L. Pereira, J. A. Hoffman, B. R. Shy, C. M. Yuen, D. R. Liu, and B. J. Merrill. 2011. "Opposing effects of Tcf3 and Tcf1 control Wnt stimulation of embryonic stem cell self-renewal." *Nat Cell Biol* 13 (7): 762-70. https://doi.org/10.1038/ncb2283. http://dx.doi.org/10.1038/ncb2283.

Ying, Q. L., J. Wray, J. Nichols, L. Batlle-Morera, B. Doble, J. Woodgett, P. Cohen, and A. Smith. 2008. "The ground state of embryonic stem cell self-renewal." *Nature* 453 (7194): 519-23. https://doi.org/10.1038/nature06968. http://dx.doi.org/10.1038/nature06968.

Yost, C., M. Torres, J. R. Miller, E. Huang, D. Kimelman, and R. T. Moon. 1996. "The axis-inducing activity, stability, and subcellular distribution of beta-catenin is regulated in Xenopus embryos by glycogen synthase kinase 3." *Genes Dev* 10 (12): 1443-54. https://doi.org/10.1101/gad.10.12.1443. https://www.ncbi.nlm.nih.gov/pubmed/8666229.

Zhang, X., K. A. Peterson, X. S. Liu, A. P. McMahon, and S. Ohba. 2013. "Gene regulatory networks mediating canonical Wnt signal-directed control of pluripotency and differentiation in embryo stem cells." *Stem Cells* 31 (12): 2667-79.

Figure Legends

Figure 1. NPEM supplemented with differential levels of CHIR99021 models nephron progenitor cell maintenance or differentiation in a plate. (A) Immuno-fluorescence (IF) staining showing expression level of Six2, non-phospho (NP) β-catenin and Jag1 in NPC cultured in NPEM supplemented with various CHIR dosages. (B) Relative intensity of IF signals from individual cells in experiment associated with A. (C) Heatmap/Hierarchical cluster of expression levels of NPC signature, self-renewal and differentiation marker genes. (D) Top 5 enriched GO terms of indicated differentially expressed gene lists, analyzed by DAVID.

Link to high-definition figure: https://www.dropbox.com/s/76chyrs07m0toen/Fig%201.pdf?dl=0

Figure 1-figure supplement 1. Supplementary RNA-Seq data analysis. (A) Overview of experiment design and data available (grey). (B) Bar plots show RT-qPCR measurement of relative expression of the indicated genes, as verification of results in Fig. 1C. (C) Hierarchical cluster of R-square values between transcriptome-wide TPM of the indicated pair of replicate RNA-Seq data sets. (D) Top 5 enriched GO

terms of genes differentially expressed between low CHIR condition and uncultured NPC. (E) Top 5 enriched GO terms of genes differentially expressed between low CHIR and no CHIR conditions. (F) Venn diagram shows overlap of β-catenin target genes with all genes associated the gene ontology term 'cell cycle' that are highly expressed in low CHIR vs. no CHIR condition. (G) Heatmap and hierarchical cluster showing log2 relative TPM (TPM divided by mean across samples) to reflect change of gene expression (at isoform level) of Karner et al., 2011 class II genes (differentially expressed low CHIR > no CHIR or high CHIR > low CHIR) in our data set. The highlighted gene is supported by genetic evidence of regulation by β-catenin in the current data. (H) Immuno-fluorescence (IF) staining of SIX2 in unpurified NFC cells and NPC freshly purified from NFC; bar plots showing percentage of SIX2+ cells in the preps.

Figure 2. High dosage of CHIR99021 triggered change of NPC epigenome. (A and B) Genome browser view of RNA-Seq, ATAC-Seq, as well as Six2, H3K27ac, H3K27me3 and Ser5P ChIP-Seq data near *Six2* (A) and *Wnt4* (B) in low CHIR (left) and high CHIR (right) conditions. Black Arrow indicates Six2DE, Wnt4DE, respectively. (C) Display of differentially accessible regions (DARs) generated by the indicated comparisons. (Left) Heatmaps showing log2 normalized read counts of top 500 most significant DARs; (middle) Top 5 most significant gene ontology terms associated with the DARs; (right) Top 5 most enriched motifs discovered *de novo* in the DARs; * indicate less well conserved motifs for the factor.

Figure 2-figure supplement 1. Supplementary ATAC-Seq data analysis. (A) Hierarchical cluster of R-square values between normalized ATAC-Seq reads within merged peaks from all samples. (B) Histograms of distances from differentially accessible (DA) chromatin regions to TSS implicate a predominant enhancer feature.

Figure 3. Differential expression of TCF/LEF family transcription factors in NPC in response to distinct level of CHIR. (A) Bar plots showing RNA-Seq measured expression levels of TCF/LEF family factors in NPC cultured in NPEM culture supplemented with various concentration of CHIR. (B) Immuno-fluorescence (IF) staining of TCF/LEF family factors in NPEM cultured with conditions indicated. (C) Relative intensity of IF signals from individual cells in experiment associated with B. Link to high-definition figure: https://www.dropbox.com/s/pvhu1ffhoujt39p/Fig%203.pdf?dl=0

Figure 3-figure supplement 1. Supplementary evidence for differential expression of TCF/LEF factors. (A) Bar plots show RT-qPCR measurement of relative expression of TCF/LEF family factors, as verification for results in Fig. 3A. (B) Bar plots show expression of individual transcripts of TCF/LEF

factors in our RNA-Seq data. (C) tSNE plot displaying unbiased cluster of nephron lineage cells profiled by single-cell RNA-Seq. (D) Feature plots displaying distribution of self-renewal (red) and differentiation (green) marker genes transcripts on the tSNE plot. (E) Feature plots showing distribution of TCF/LEF factors transcripts on the tSNE plot. (F) Dot plots showing accumulated expression level of marker genes as well as TCF/LEF factor in selected clusters of cells.

Figure 3-figure supplement 2. Expression of TCF/LEF factors measured by immunoblots. (A) Immunoblots of TCF/LEF family factors in NPC cultured in NPEM with the indicated treatment; red arrows indicate target band. (B) Quantification of target band intensity normalized to histone H3 intensity.

Figure 4. Increased CHIR dosage induces a switch of TCF/LEF factors binding to the genome. (A and B) Genome browser view of *Wnt4* enhancer locus showing ChIP-Seq signal of TCF/LEF factors in low and high CHIR conditions. (C) Histograms showing binding intensity of TCF/LEF factors and chromatin markers on the 3 sets of TCF/LEF binding sites assigned by overlap of low CHIR Tcf7l1 and high CHIR Lef1 binding sites. (D) Result from de novo motif discovery of the 3 sets of TCF/LEF binding sites described in A. (E) Top Gene Ontology terms associated with the corresponding sets of TCF/LEF binding sites shown in B. (F) Percentage of TCF/LEF target genes belonging to different sets in differential expressed genes specific to low CHIR or high CHIR conditions as described in Fig. 1. (G) Venn diagram showing overlap of set 2 and 3 target genes assigned by GREAT (McLean et al. 2010). (H) Histograms showing quantification of reads from the indicated data sets in +/-2kb of β-catenin binding sites in high CHIR condition.

Figure 4-figure supplement 1. Supplementary ChIP-Seq data analysis. (A) Numbers of and overlap between binding sites of the same factors between different conditions. (B) Numbers of and overlap between binding sites of different factors in the same conditions. (C) Most enriched motifs by *de novo* discovery (Homer) from binding sites of the data sets indicated. (D) Hierarchical clustering of normalized read counts of ChIP-Seq data sets on merged binding sites.

Figure 4-figure supplement 2. Analysis of Tcf7l1 binding in low CHIR. (A) Overlap of direct and indirect Tcf7l1 binding in low CHIR with Lef1 binding in high CHIR (left) and enrichment of ChIP-Seq reads on the two types of binding events. (B) Distribution of ATAC-Seq, H3K27ac ChIP-Seq and Ser5P ChIP-Seq signals on Tcf7l1 binding sites in low CHIR with or without TCF/LEF motifs. (C) Gene Ontology analysis by GREAT on Tcf7l1 binding sites in low CHIR with or without TCF/LEF motifs. (D) Overlap of predicted target genes between Tcf7l1 binding sites in low CHIR with or without TCF/LEF

motifs. (E) Histograms showing intensities of ATAC-Seq or ChIP-Seq signals around set1, 2 and 3 TCF/LEF binding sites in low CHIR and high CHIR conditions.

Figure 4-figure supplement 3. β-catenin binding sites near (A) Pla2g7 and (B) Tafa5, two β-catenin target genes reported in Karner et al., 2011. The ChIP-qPCR target sites were marked as red bins on the top track. The highlighted region is where our data is consistent with Karner's.

Figure 5. β-catenin activates gene expression through both stable and *de novo* enhancer-promoter loops. (A) β-catenin binding sites that overlap with an anchor of chromatin loop in high CHIR, the proportion that connects to a TSS (grey in the pie chart) and segregation between 2 types of loops defined in B. (B) Overlap of chromatin loops between low CHIR and high CHIR conditions. (C, D, E, F) Examples (C, E) and schematics (D, F) of β-catenin utilizing low/high CHIR-shared enhancer-promoter loops to activate *Wnt4* (C, D) or high CHIR-specific loops to activate *Lef1* (E, F). Black arrow at the bottom indicates the β-catenin binding sites involved in the loops.

Figure 5-figure supplement 1. Supplementary HiC data analysis. (A) Reproducible loops between replicates. (B) Bar plots showing the percentage of loops in the corresponding category (high CHIR only, low CHIR only or share) that are linked to differentially expressed genes (DEG) that are high in low CHIR or high CHIR.

Supplementary File 1. Differentially expressed genes (DEG) between conditions.

Supplementary File 2. Differentially accessible regions (DAR) between conditions.

Supplementary File 3. Tcf7l1 and Lef1 peak coordinates by category as in Figure 4.

Supplementary File 4. HiC loops to TSS

Supplementary File 5. HiC loops that are anchored on β-catenin binding sites in high CHIR condition.

Supplementary File 6. Expression of Wnt target genes published in Karner et al., 2011

Fig. 1

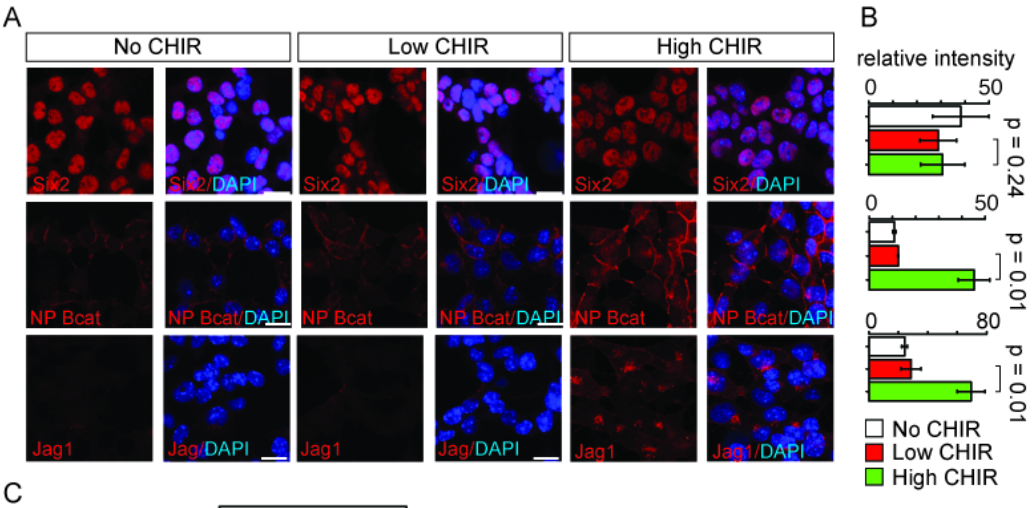

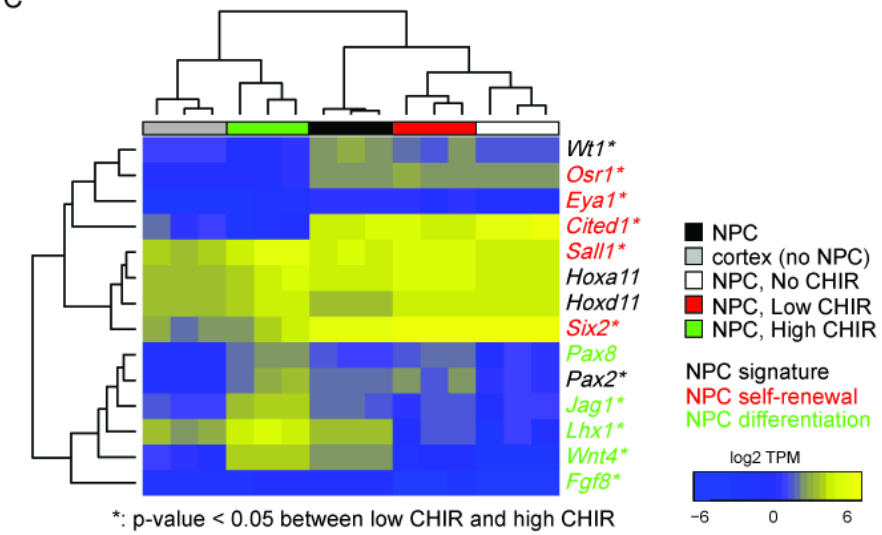

*: p-value < 0.05 between low CHIR and high CHIR

D

GO terms	#	p-adj.	F.E.
NPC > NFC: 221 transcripts			
multicellular organism development	38	6.7E-10	4.0
metanephros development	9	1.1E-6	25.6
branching involved in ureteric bud morphogenesis	9	5.2E-6	20.3
ureteric bud development	8	8.5E-5	18.0
kidney development	11	8.8E-5	9.2
High CHIR > Low CHIR: 207 transcripts			
multicellular organism development	32	6.4E-6	3.4
negative regulation of canonical Wnt signaling pathway	10	3.2E-4	10.6
embryonic limb morphogenesis	8	7.7E-4	13.7
cell differentiation	23	7.7E-4	3.2
positive regulation of cell migration	12	7.7E-4	6.4
Low CHIR > High CHIR: 153 transcripts			
metanephros development	10	2.4E-9	40.3
ureteric bud development	10	1.1E-8	31.9
kidney development	11	4.7E-6	13.0
branching involved in ureteric bud morphogenesis	8	6.8E-6	25.5
neural crest cell developmetn	5	8.6E-4	45.1

Fig. 2

A

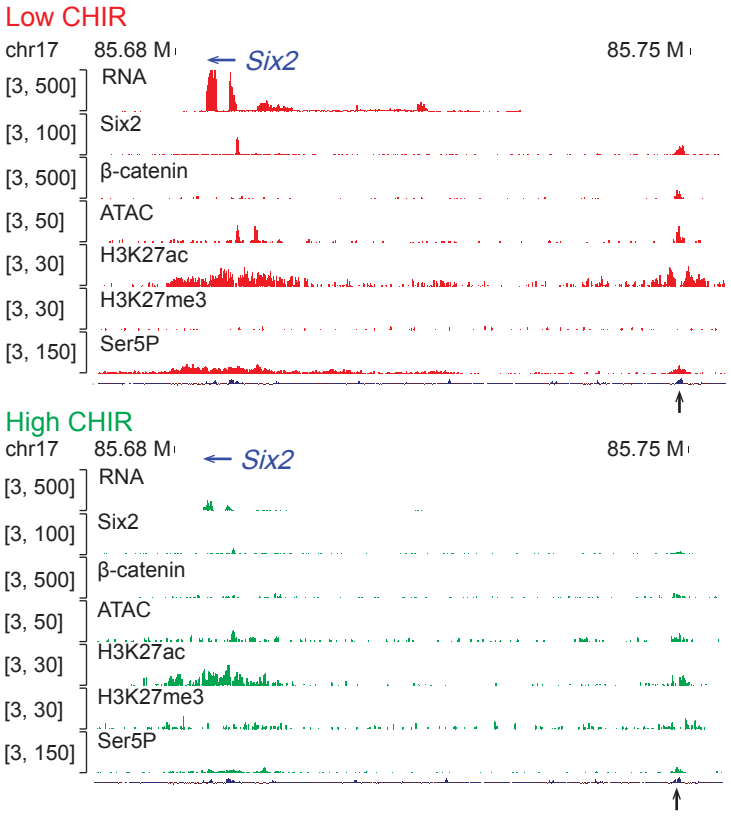

B

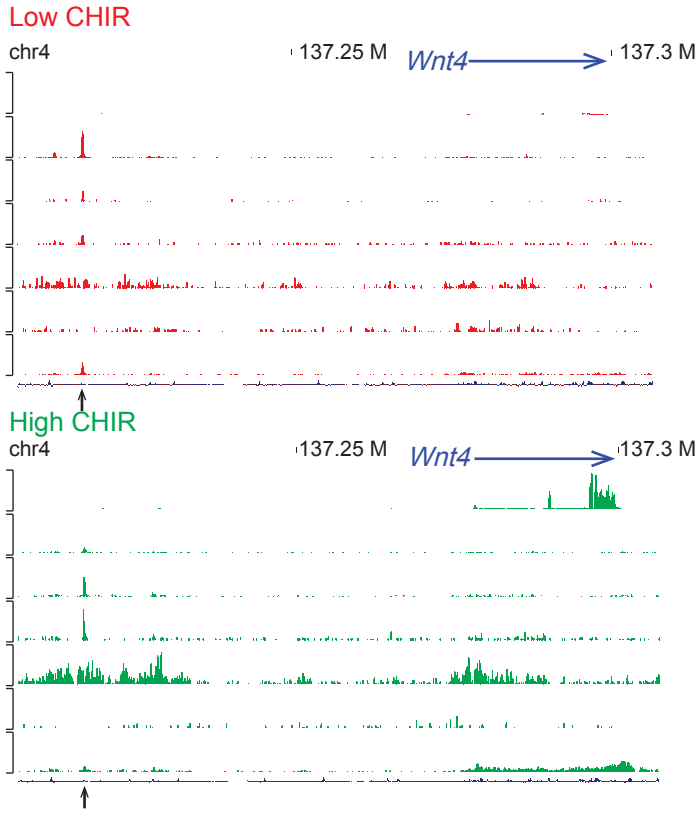

C

GO terms	p-value	f.c.	region #	gene #
NPC vs. NFC: 3,237 regions				
mesenchymal-epithelial cell signaling	2E-08	3.8	26	7
inactivation of MAPK activity	4E-07	3.7	22	10
metanephric renal vesicle morphogenesis	7E-07	3.4	23	10
positive regulation of chemotaxis	8E-07	2.0	57	22
lung cell differentiation	1E-06	2.4	40	19
High CHIR vs Low CHIR: 986 regions				
morphogenesis of embryonic epithelium	2E-09	2.7	50	37
ureteric bud development	2E-06	2.3	40	26
regulation of cellular response to growth factor stimulus	2E-06	2.3	39	25
positive regulation of cell adhesion	2E-06	2.4	37	25
positive regulation of epithelial cell proliferation	3E-06	2.3	38	23
Low CHIR vs High CHIR: 1,007 regions				
kidney development	6E-08	3.0	64	39
negative regulation of necrotic cell death	2E-06	7.2	10	5
regulation of necrotic cell death	3E-06	6.2	11	6
regulation of organ growth	3E-06	2.7	29	17
ossification	1E-05	2.1	42	27

D

motif logo	p-value	obs./bg. %	pred. TF
	1e-291	24.1/5.1	Six2
	1e-105	6.5/0.9	Hox11
	1e-53	15/7.1	Pax
	1e-51	2.8/0.3	Hox
	1e-35	6.1/2.2	Wt1
	1e-180	22.0/1.4	Jun
	1e-145	20.1/1.7	Tcf/Lef
	1e-39	12.5/3.0	Hox*
	1e-15	2.7/0.3	Runx
	1e-53	29.8/11.6	Six2
	1e-51	19.4/5.6	Fox
	1e-39	17.8/5.8	Hox*
	1e-24	22.6/11.2	Hox
	1e-18	38.4/25.5	Wt1*

Fig. 3

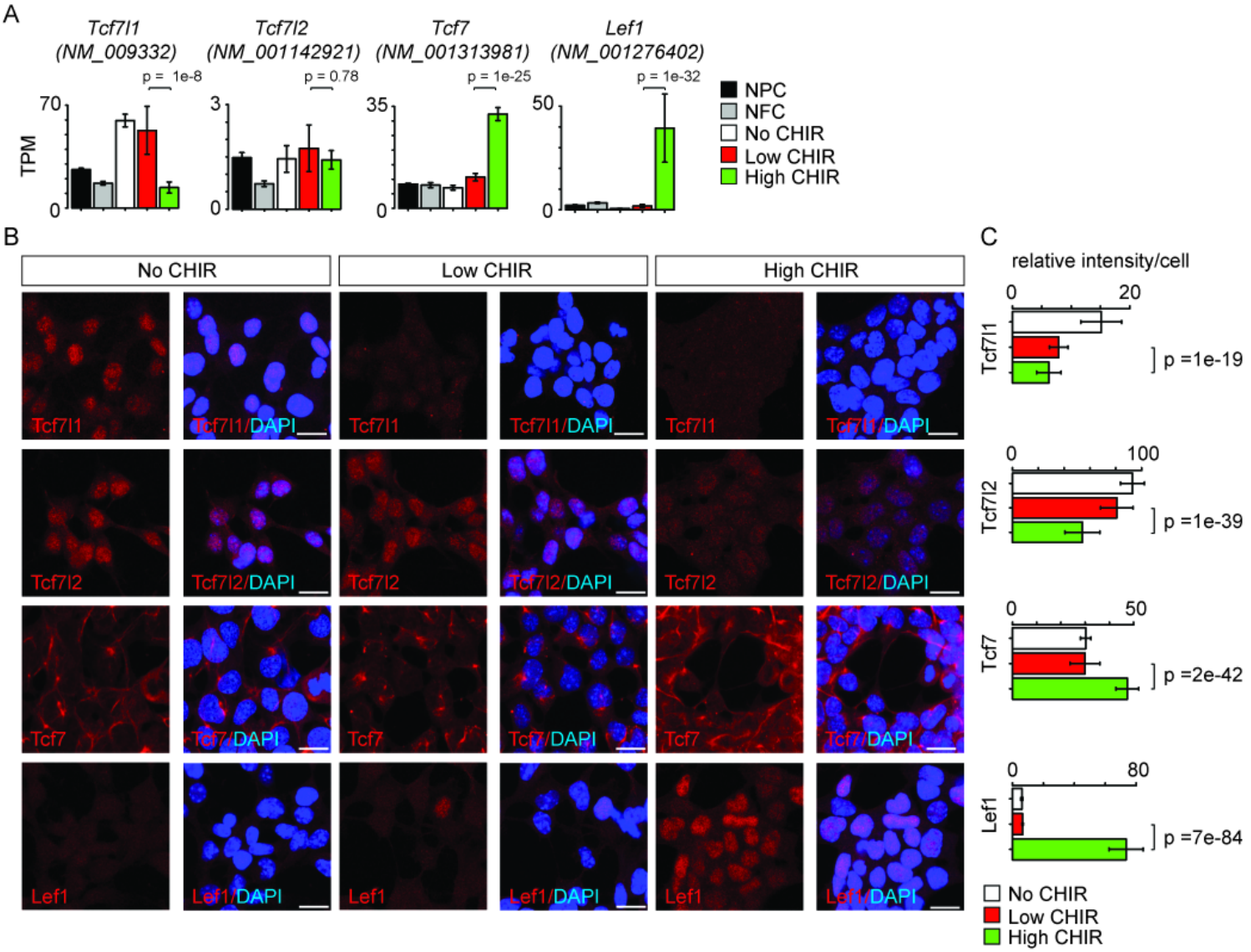

Fig. 4

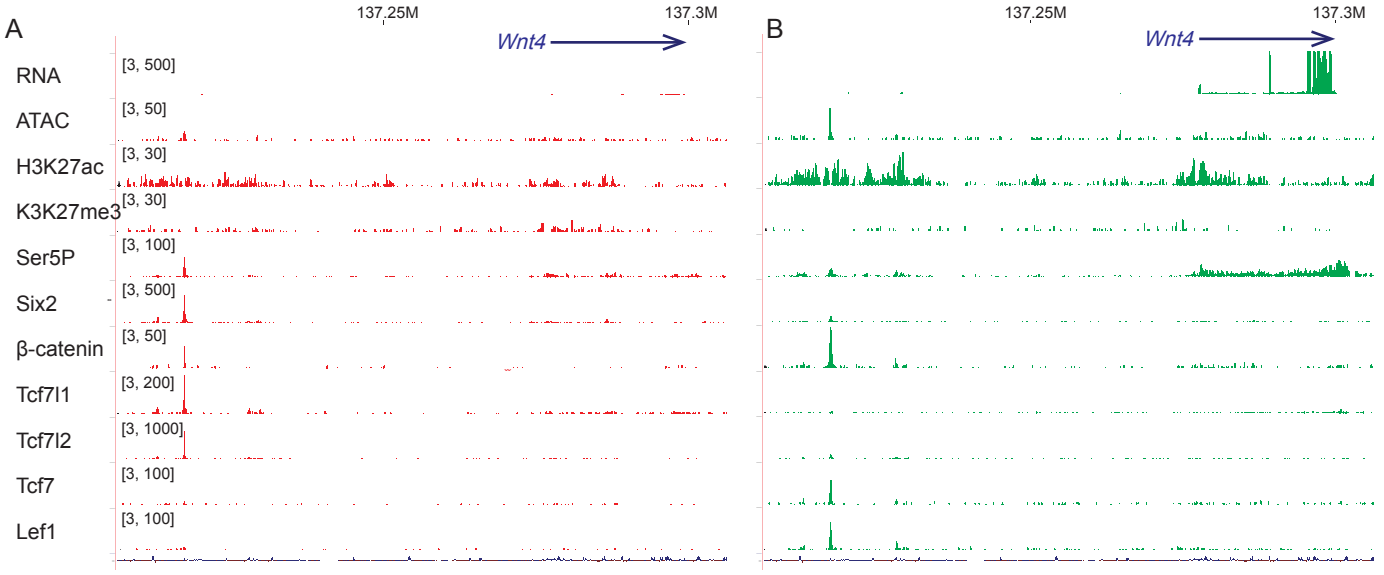

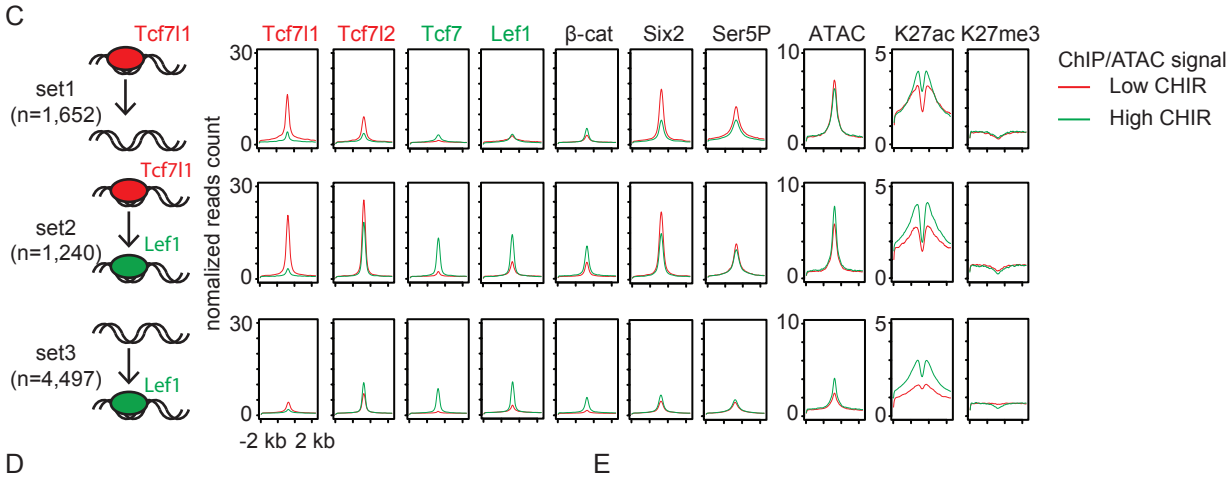

D

	motif logo	pred. TF	p-value	obs./bg.%
set1 (n=1,652)		Irf4*	1e-137	3.6/0.1
		Hox	1e-79	14.9/4.9
		Runx*	1e-59	1.0/0.0
		Klf7*	1e-57	1.8/0.0
		Myb*	1e-38	0.7/0.0
set2 (n=1,240)		Tcf/Lef	1e-468	29.8/2.4
		Nkx/Hox	1e-141	15.1/2.5
		Coup-TFII	1e-68	21.6/8.9
		Hnf4a*	1e-32	0.8/0.0
		Hox	1e-28	4.9/1.3
set3 (n=4,497)		Tcf/Lef	1e-4004	39.0/1.7
		Nkx/Hox	1e-248	17.9/7.5
		Runx	1e-164	7.4/2.2
		Pbx/Jun	1e-135	14.4/7.2
		Ctcf	1e-54	1.7/0.4

E

GO terms	p-value	# genes
metanephric nephron morphogenesis	1E-23	41
metanephric renal vesicle morphogenesis	2E-21	33
renal vesicle morphogenesis	8E-21	33
metanephros morphogenesis	3E-20	43
renal vesicle development	3E-19	35
renal vesicle morphogenesis	2E-13	22
paramesonephric duct development	4E-12	11
renal vesicle development	5E-12	23
epithelial tube morphogenesis	7E-12	108
metanephric nephron morphogenesis	2E-11	23
Wnt receptor signaling pathway	3E-23	224
morphogenesis of embryonic epithelium	1E-20	185
embryonic epithelial tube formation	6E-18	155
epithelial tube formation	2E-17	155
tube formation	8E-17	167

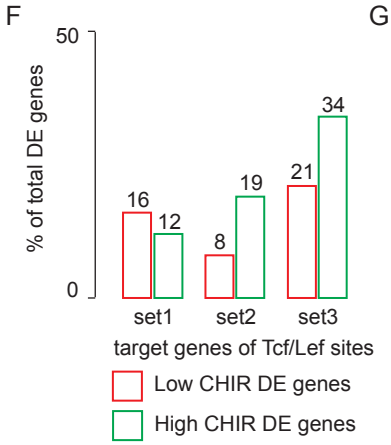

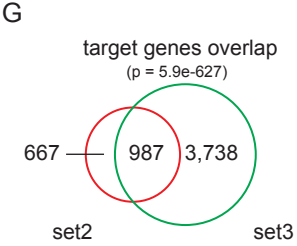

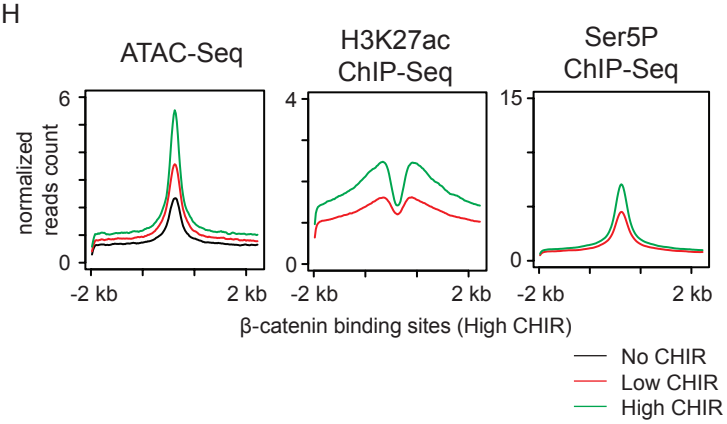

Fig. 5

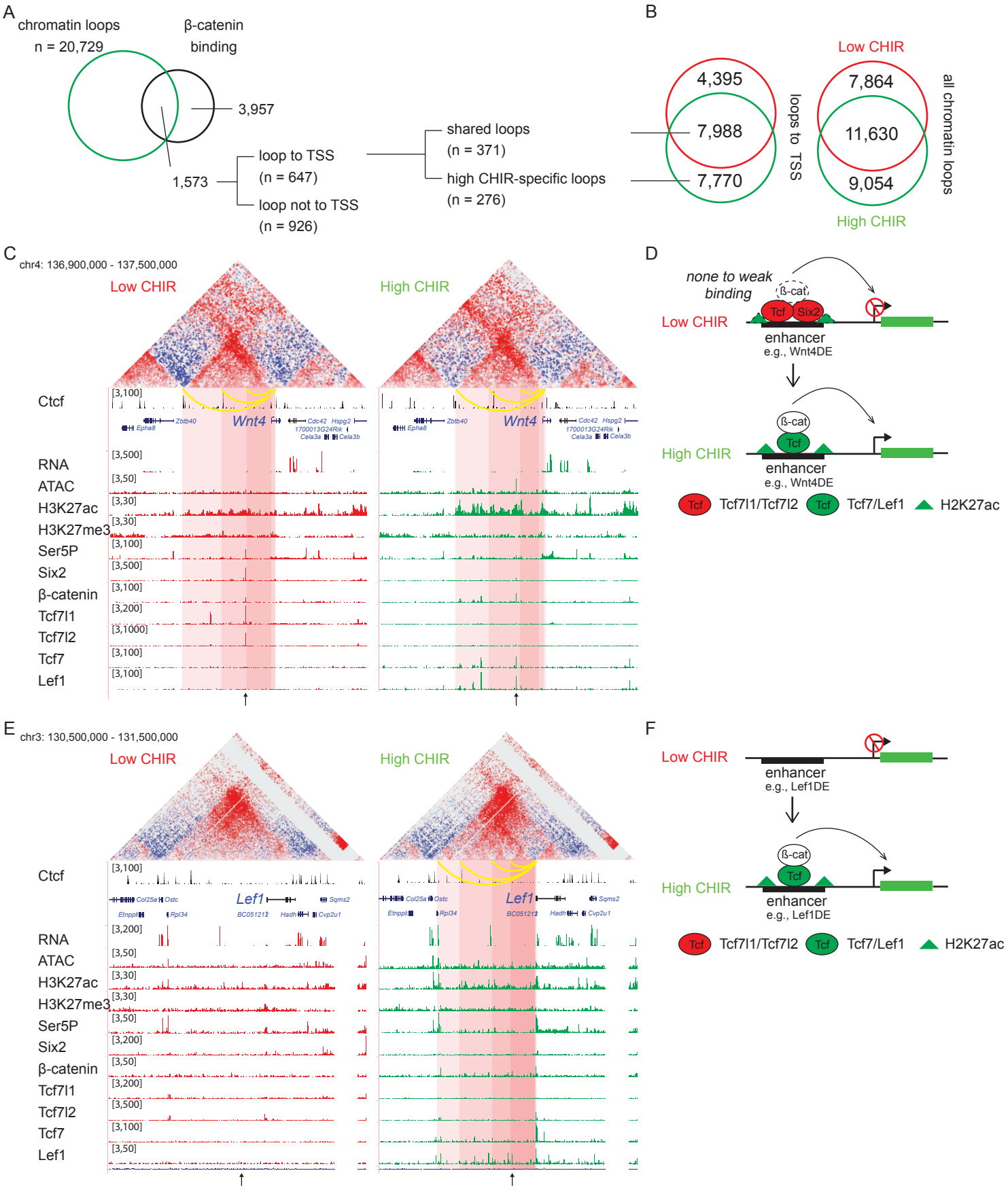
A
chromatin loops
n = 20,729
β-catenin
binding
3,957
1,573
loop to TSS
(n = 647)
loop not to TSS
(n = 926)
shared loops
(n = 371)
high CHIR-specific loops
(n = 276)
B
Low CHIR
4,395
7,988
7,770
loops to TSS
7,864
11,630
9,054
all chromatin loops
High CHIR
C
chr4: 136,900,000 - 137,500,000
Low CHIR
High CHIR
Ctcf
Wnt4
RNA
ATAC
H3K27ac
H3K27me3
Ser5P
Six2
β-catenin
Tcf7l1
Tcf7l2
Tcf7
Lef1
D
none to weak
binding
ß-cat
Tcf
Six2
Low CHIR
enhancer
e.g., Wnt4DE
High CHIR
Tcf7l1/Tcf7l2
Tcf7/Lef1
H2K27ac
E
chr3: 130,500,000 - 131,500,000
Low CHIR
High CHIR
Ctcf
Lef1
RNA
ATAC
H3K27ac
H3K27me3
Ser5P
Six2
β-catenin
Tcf7l1
Tcf7l2
Tcf7
Lef1
F
Low CHIR
enhancer
e.g., Lef1DE
High CHIR
Tcf7l1/Tcf7l2
Tcf7/Lef1
H2K27ac

Fig. 1S1

A

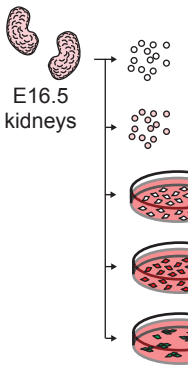

	RNA-Seq	ATAC-Seq	H3K27ac ChIP-Seq	H3K27me3 ChIP-Seq	Ser5P ChIP-Seq	β-catenin ChIP-Seq	Six2 ChIP-Seq	Tcf7l1 ChIP-Seq	Tcf7l2 ChIP-Seq	Tcf7 ChIP-Seq	Lef1 ChIP-Seq
NPC	3	3	2			2	2	2	2	2	2
NPC-free cortex (NFC)	3	3									
No CHIR (0 uM)	3	3									
Low CHIR (1.25 uM CHIR)	3	3	2	2	2	2	2	2	2	2	2
High CHIR (5 uM CHIR)	3	3	2	2	2	2	2	2	2	2	2

B

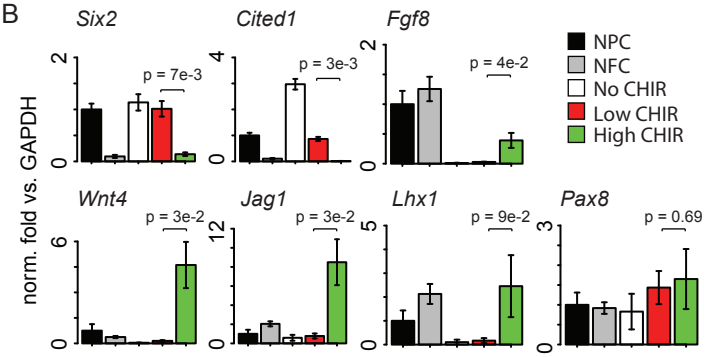

C

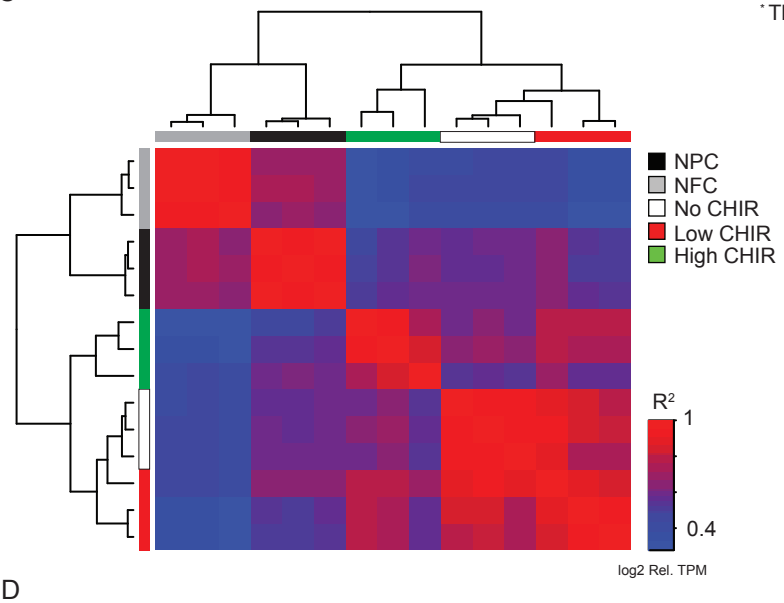

D

GO terms	#	p-adj	F.E.
Low CHIR > NPC (511 transcripts)			
sterol biosynthetic process	16	3.0E-15	29.1
cholesterol biosynthetic process	16	1.5E-14	24.6
steroid metabolic process	17	8.9E-9	9.9
lipid metabolic process	35	4.9E-8	3.7
steroid biosynthetic process	14	1.3E-7	11.1
NPC > Low CHIR (283 transcripts)			
response to mechanical stimulus	11	6.7E-6	14.3
multicellular organism development	34	1.7E-4	2.7
skeletal muscle cell differentiation	9	1.7E-4	13.4
positive regulation of transcription from RNA polymerase II promoter	32	5.2E-4	2.6
positive regulation of transcription, DNA-templated	23	6.9E-4	3.3

E

GO terms	#	p-adj	F.E
Low CHIR > No CHIR (405 transcripts*)			
cell cycle	95	2.1E-61	9.2
cell division	75	1.1E-55	12.0
mitotic nuclear division	66	1.3E-53	14.2
chromosome segregation	27	6.6E-23	18.1
DNA replication	26	8.1E-18	12.6
No CHIR > Low CHIR (201 transcripts*)			
organ regeneration	7	1.3E-2	14.0
cell adhesion	16	1.8E-2	3.7
skeletal system morphogenesis	6	4.9E-2	12.5
response to estradiol	7	9.0E-2	7.8
positive regulation of apoptotic process	9	2.1E-1	3.7

* These DE trancripts were identified with a different DE threshold (Table S1).

F

G

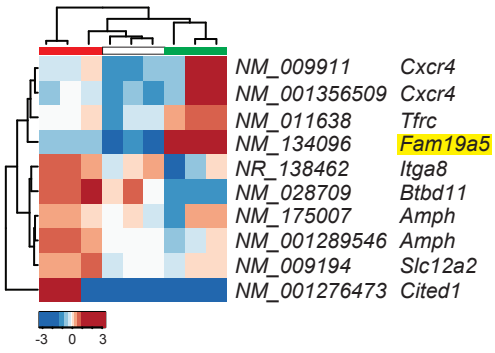

H

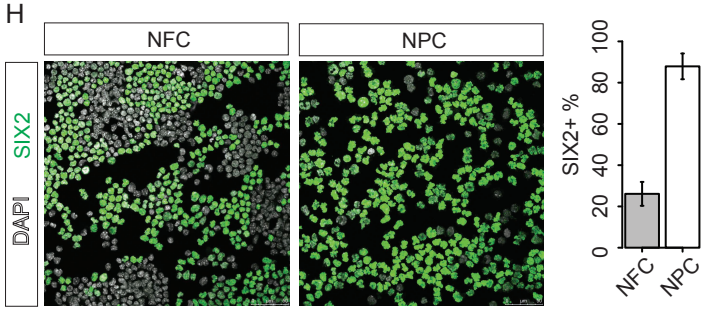

Fig. 2S1

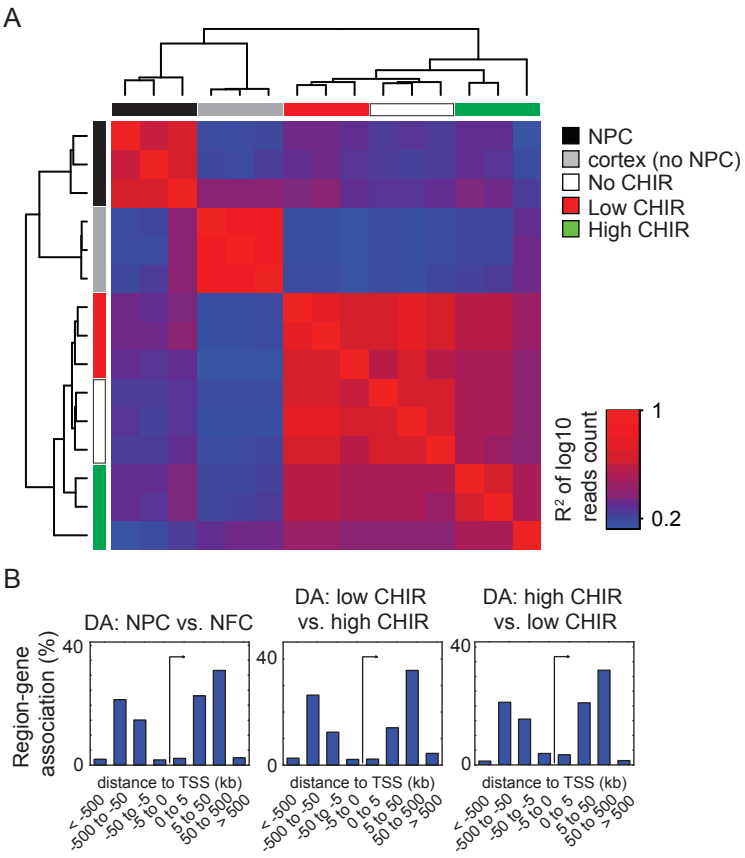
A
NPC
cortex (no NPC)
No CHIR
Low CHIR
High CHIR
R² of log10 reads count
1
0.2
B
DA: NPC vs. NFC
DA: low CHIR vs. high CHIR
DA: high CHIR vs. low CHIR
Region-gene association (%)
40
0
distance to TSS (kb)
< -500
-500 to -50
-50 to -5
-5 to 0
0 to 5
5 to 50
50 to 500
> 500

Fig. 3S1

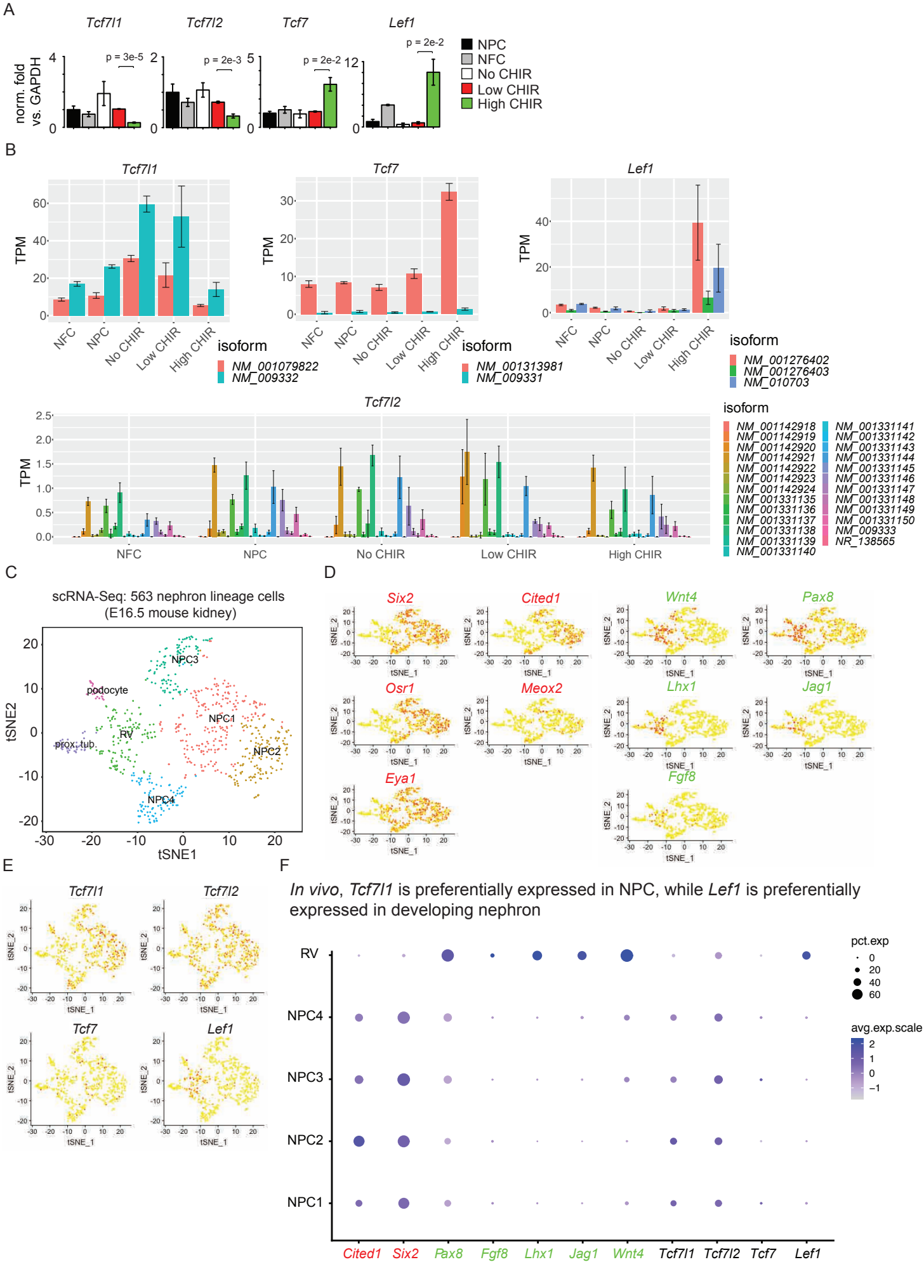
A
Tcf7l1
Tcf7l2
Tcf7
Lef1
norm. fold vs. GAPDH
p = 3e-5
p = 2e-3
p = 2e-2
p = 2e-2
NPC
NFC
No CHIR
Low CHIR
High CHIR
B
TPM
isoform
NM_001079822
NM_009332
NM_001313981
NM_009331
NM_001276402
NM_001276403
NM_010703
NM_001142918
NM_001142919
NM_001142920
NM_001142921
NM_001142922
NM_001142923
NM_001142924
NM_001331135
NM_001331136
NM_001331137
NM_001331138
NM_001331139
NM_001331140
NM_001331141
NM_001331142
NM_001331143
NM_001331144
NM_001331145
NM_001331146
NM_001331147
NM_001331148
NM_001331149
NM_001331150
NM_009333
NR_138565
C
scRNA-Seq: 563 nephron lineage cells
(E16.5 mouse kidney)
NPC3
podocyte
NPC1
RV
prox. tub.
NPC2
NPC4
tSNE1
tSNE2
D
Six2
Cited1
Wnt4
Pax8
Osr1
Meox2
Lhx1
Jag1
Eya1
Fgf8
tSNE_1
tSNE_2
E
Tcf7l1
Tcf7l2
Tcf7
Lef1
F
In vivo, Tcf7l1 is preferentially expressed in NPC, while Lef1 is preferentially expressed in developing nephron
RV
NPC4
NPC3
NPC2
NPC1
Cited1
Six2
Pax8
Fgf8
Lhx1
Jag1
Wnt4
Tcf7l1
Tcf7l2
Tcf7
Lef1
pct.exp
avg.exp.scale

Fig. 2S2

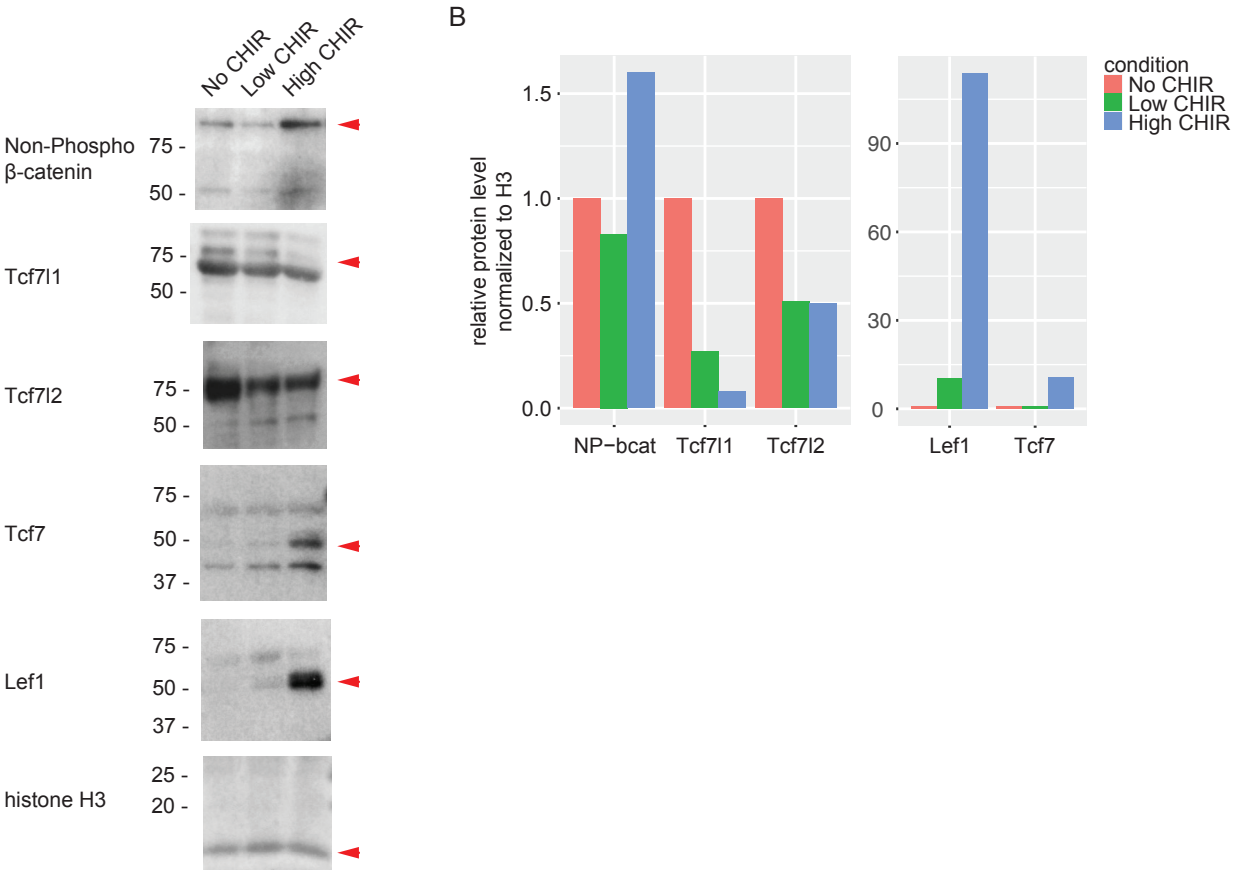
A
No CHIR
Low CHIR
High CHIR
Non-Phospho β-catenin
75 -
50 -
Tcf7l1
75 -
50 -
Tcf7l2
75 -
50 -
Tcf7
75 -
50 -
37 -
Lef1
75 -
50 -
37 -
histone H3
25 -
20 -
B
relative protein level normalized to H3
1.5
1.0
0.5
0.0
NP−bcat
Tcf7l1
Tcf7l2
90
60
30
0
Lef1
Tcf7
condition
No CHIR
Low CHIR
High CHIR

Fig. 4S1

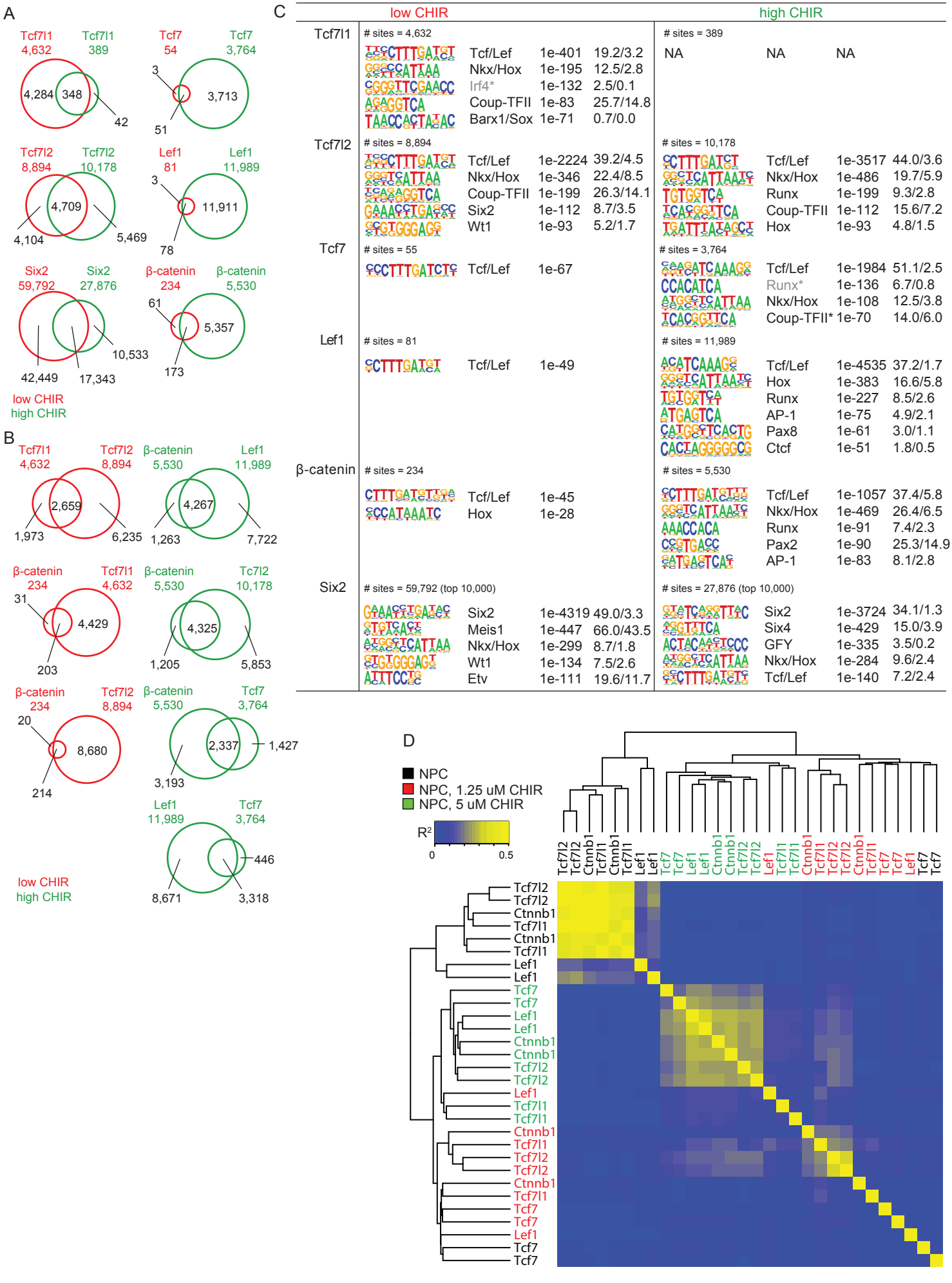
A
Tcf7l1 4,632
Tcf7l1 389
4,284
348
42
Tcf7 54
Tcf7 3,764
3
3,713
51
Tcf7l2 8,894
Tcf7l2 10,178
4,709
4,104
5,469
Lef1 81
Lef1 11,989
3
11,911
78
Six2 59,792
Six2 27,876
10,533
42,449
17,343
β-catenin 234
β-catenin 5,530
61
5,357
173
low CHIR
high CHIR
B
Tcf7l1 4,632
Tcf7l2 8,894
2,659
1,973
6,235
β-catenin 5,530
Lef1 11,989
4,267
1,263
7,722
β-catenin 234
Tcf7l1 4,632
31
4,429
203
β-catenin 5,530
Tc7l2 10,178
4,325
1,205
5,853
β-catenin 234
Tcf7l2 8,894
20
8,680
214
β-catenin 5,530
Tcf7 3,764
2,337
1,427
3,193
Lef1 11,989
Tcf7 3,764
446
8,671
3,318
low CHIR
high CHIR
C
low CHIR
high CHIR
Tcf7l1
sites = 4,632
Tcf/Lef 1e-401 19.2/3.2
Nkx/Hox 1e-195 12.5/2.8
Irf4* 1e-132 2.5/0.1
Coup-TFII 1e-83 25.7/14.8
Barx1/Sox 1e-71 0.7/0.0
sites = 389
NA NA NA
Tcf7l2
sites = 8,894
Tcf/Lef 1e-2224 39.2/4.5
Nkx/Hox 1e-346 22.4/8.5
Coup-TFII 1e-199 26.3/14.1
Six2 1e-112 8.7/3.5
Wt1 1e-93 5.2/1.7
sites = 10,178
Tcf/Lef 1e-3517 44.0/3.6
Nkx/Hox 1e-486 19.7/5.9
Runx 1e-199 9.3/2.8
Coup-TFII 1e-112 15.6/7.2
Hox 1e-93 4.8/1.5
Tcf7
sites = 55
Tcf/Lef 1e-67
sites = 3,764
Tcf/Lef 1e-1984 51.1/2.5
Runx* 1e-136 6.7/0.8
Nkx/Hox 1e-108 12.5/3.8
Coup-TFII* 1e-70 14.0/6.0
Lef1
sites = 81
Tcf/Lef 1e-49
sites = 11,989
Tcf/Lef 1e-4535 37.2/1.7
Hox 1e-383 16.6/5.8
Runx 1e-227 8.5/2.6
AP-1 1e-75 4.9/2.1
Pax8 1e-61 3.0/1.1
Ctcf 1e-51 1.8/0.5
β-catenin
sites = 234
Tcf/Lef 1e-45
Hox 1e-28
sites = 5,530
Tcf/Lef 1e-1057 37.4/5.8
Nkx/Hox 1e-469 26.4/6.5
Runx 1e-91 7.4/2.3
Pax2 1e-90 25.3/14.9
AP-1 1e-83 8.1/2.8
Six2
sites = 59,792 (top 10,000)
Six2 1e-4319 49.0/3.3
Meis1 1e-447 66.0/43.5
Nkx/Hox 1e-299 8.7/1.8
Wt1 1e-134 7.5/2.6
Etv 1e-111 19.6/11.7
sites = 27,876 (top 10,000)
Six2 1e-3724 34.1/1.3
Six4 1e-429 15.0/3.9
GFY 1e-335 3.5/0.2
Nkx/Hox 1e-284 9.6/2.4
Tcf/Lef 1e-140 7.2/2.4
D
NPC
NPC, 1.25 uM CHIR
NPC, 5 uM CHIR
R2
0
0.5
Tcf7l2 Tcf7l2 Ctnnb1 Tcf7l1 Ctnnb1 Tcf7l1 Lef1 Lef1 Tcf7 Tcf7 Lef1 Lef1 Ctnnb1 Ctnnb1 Tcf7l2 Tcf7l2 Lef1 Tcf7l1 Tcf7l1 Ctnnb1 Tcf7l1 Tcf7l2 Tcf7l2 Ctnnb1 Tcf7l1 Tcf7 Tcf7 Lef1 Tcf7 Tcf7
Tcf7l2
Tcf7l2
Ctnnb1
Tcf7l1
Ctnnb1
Tcf7l1
Lef1
Lef1
Tcf7
Tcf7
Lef1
Lef1
Ctnnb1
Ctnnb1
Tcf7l2
Tcf7l2
Lef1
Tcf7l1
Tcf7l1
Ctnnb1
Tcf7l1
Tcf7l2
Tcf7l2
Ctnnb1
Tcf7l1
Tcf7
Tcf7
Lef1
Tcf7
Tcf7

Fig. 4S2

A

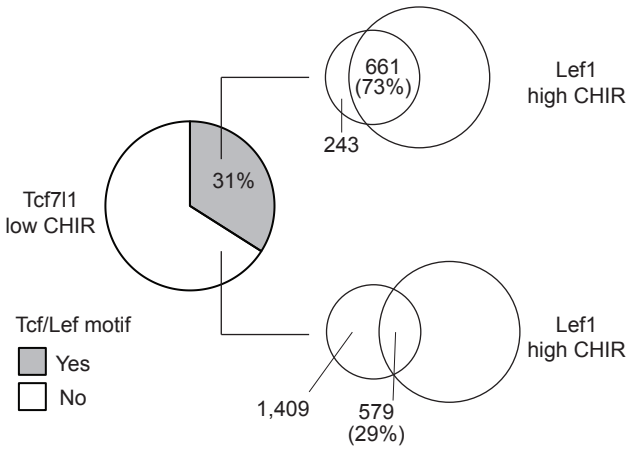

B

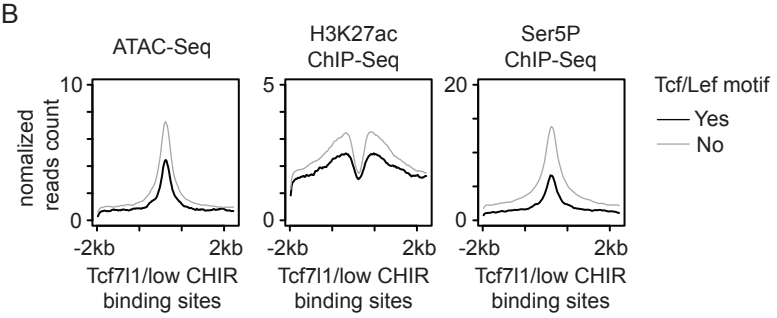

D

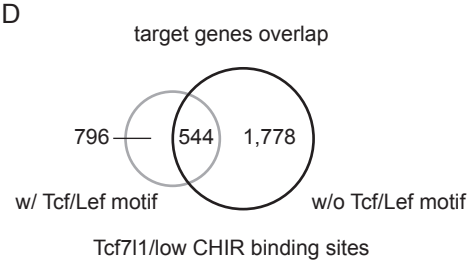

C

	GO terms	FDR
Tcf7l1/low CHIR w/ Tcf/Lef motif	renal vesicle morphogenesis	4.35E-15
	kidney development	6.43E-14
	renal vesicle development	7.11E-14
	tube development	1.09E-13
	metanephric renal vesicle morphogenesis	1.9
Tcf7l1/low CHIR w/o Tcf/Lef motif	metanephric nephron morphogenesis	1.63E-21
	renal vesicle morphogenesis	2.27E-19
	metanephric renal vesicle morphogenesis	3.8
	metanephros morphogenesis	4.99E-18
	renal vesicle development	1.21E-17

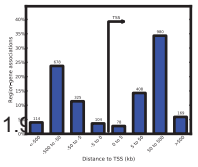

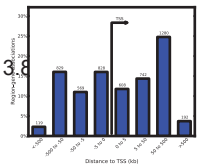

motif logo	p-value	%	pred. TF
	1e-647	93%	Tcf3
	1e-44	16%	Hox
	1e-23	23%	EAR2 (NR)
	1e-20	51%	NR class
	1e-13	18%	ETS
	1e-166	23%	NKX6-2
	1e-125	4%	Irf4
	1e-88	3%	Nkx2.2
	1e-71	2%	MZF1
	1e-65	36%	COUP-TFII (NR)

E

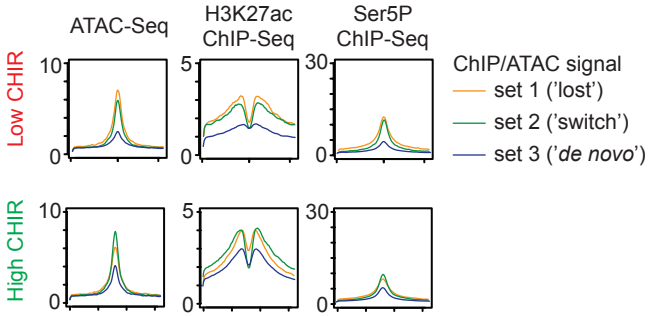

Fig. 4S3

A

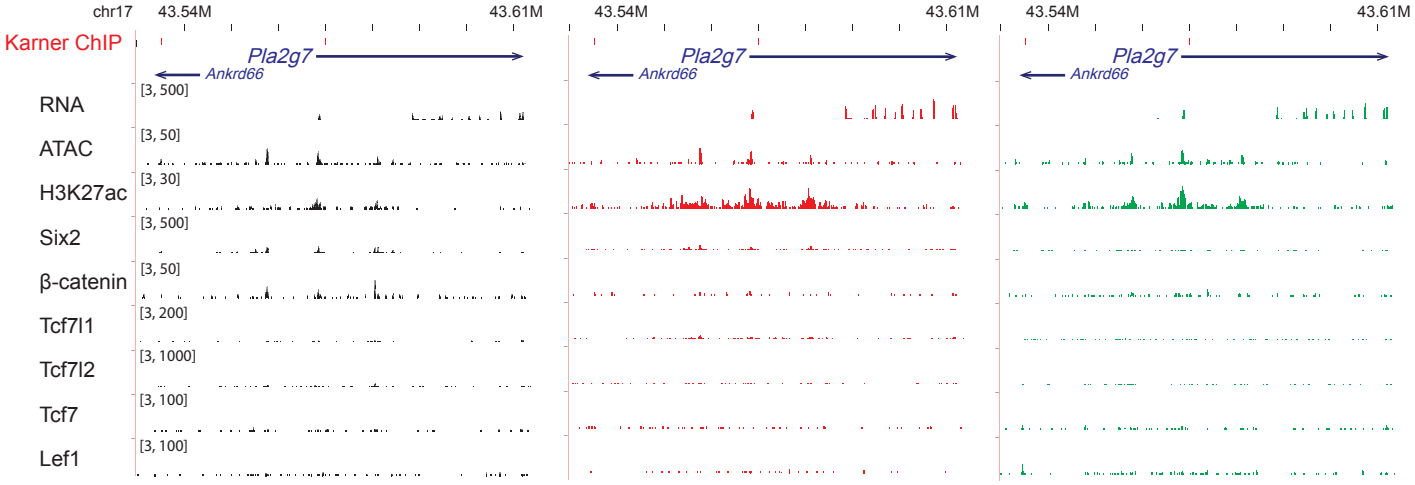
chr17
43.54M
43.61M
Karner ChIP
Pla2g7
Ankrd66
RNA
ATAC
H3K27ac
Six2
β-catenin
Tcf7l1
Tcf7l2
Tcf7
Lef1
[3, 500]
[3, 50]
[3, 30]
[3, 500]
[3, 50]
[3, 200]
[3, 1000]
[3, 100]
[3, 100]

B

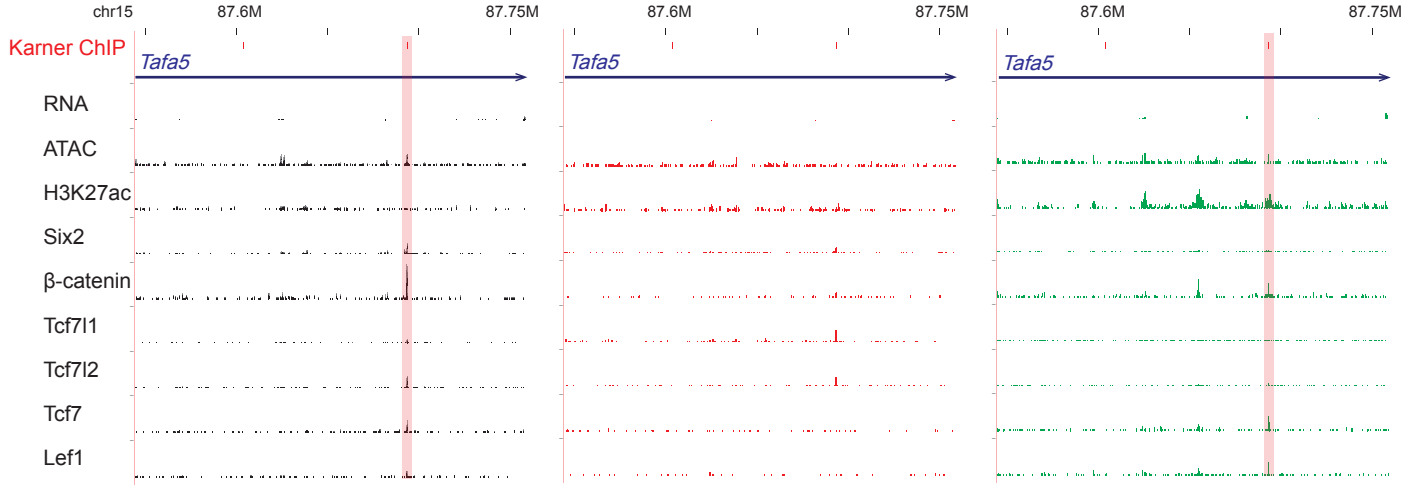
chr15
87.6M
87.75M
Karner ChIP
Tafa5
RNA
ATAC
H3K27ac
Six2
β-catenin
Tcf7l1
Tcf7l2
Tcf7
Lef1

Fig. 5S1

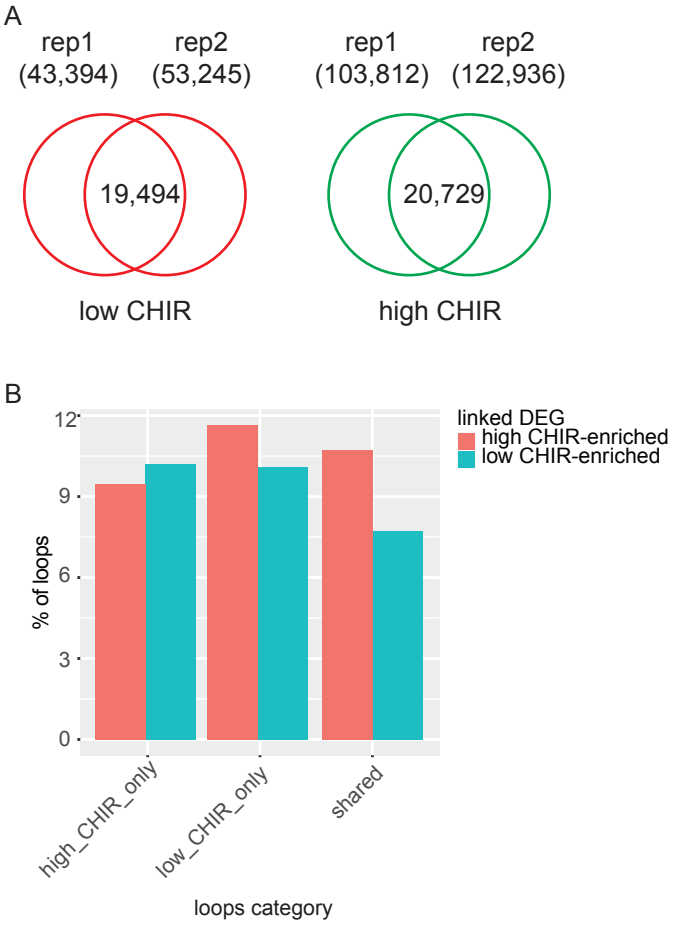
A
rep1
(43,394)
rep2
(53,245)
19,494
low CHIR
rep1
(103,812)
rep2
(122,936)
20,729
high CHIR
B
linked DEG
high CHIR-enriched
low CHIR-enriched
% of loops
12
9
6
3
0
high_CHIR_only
low_CHIR_only
shared
loops category